Elasticity of disordered nematic liquid-crystalline gels(Dissertation_全文)

AUTHOR(S):

Uchida, Nariya

CITATION:

Uchida, Nariya. Elasticity of disordered nematic liquid-crystalline gels. 京都大学, 2000, 博士(理学)

ISSUE DATE:

2000-03-23

URL:

https://doi.org/10.11501/3167080

学位申請論文

内田 就也

Elasticity of disordered nematic liquid-crystalline gels

Nariya Uchida

主論文

Thesis

Elasticity of disordered nematic liquid-crystalline gels

Nariya Uchida

Department of Physics, Kyoto University

January 31, 2000

Publication

Part of the contents of this thesis has previously been published :

Nariya Uchida and Akira Onuki,
"Elastic interactions in nematic elastomers and gels",
Europhysics Letters **45**, 341-347 (1999).

Nariya Uchida,
"Elastic effects in disordered nematic networks",
Physical Review E **60**, R13-R16 (1999).

A short summary has been submitted for publication :

Nariya Uchida,
"Anomalous elasticity of disordered nematic gels",
AIP Proceedings of the 3rd Tohwa University International Conference on Statistical Physics (November 1999, Fukuoka).

Contents

Chapter 1

Introduction

Polymer gels and rubbers constitute a unique class of condensed matter that is different from any of liquids, crystalline solids, and glasses. They are not like liquids as they show elastic responses to mechanical perturbations. They are not like crystals in that the positions of their building units have no long-range correlation. They are also distinct from ordinary glasses because large thermal fluctuations are present in gels, which are the sources of rubber elasticity. Yet, gels have some qualitative similarity to fluids near the glass transition; both of them contain structural heterogeneity on many length-scales, which are considered to produce random internal stresses [1]. One type of spatial heterogeneities in gels is that of the crosslink density. Experimentally, it is manifested as speckles in light scattering intensity, and as the "abnormal butterfly" pattern observed by small-angle neutron scattering [2]. Another type of heterogeneity is provided by random shear deformations of network meshes, which are also frozen at the moment of crosslinking.

The effect of these quenched randomnesses becomes particularly evident when we introduce some other soft order into gels. This is indeed possible, for example, by weaving liquid-crystalline polymers (LCPs) into networks. The first sample of nematic elastomers (dry gels) was synthesized by Finkelmann et al. [3] in 1981. Today there exist nematic and smectic gels as well as many of their chiral families, both dry and swollen [4]. It is also possible to crosslink block-copolymers to obtain mesoscopically ordered networks. In this thesis, we shall focus our attention on nematic gels, which have the highest and simplest symmetry among the mesophase networks. Theoretically, nematic gels are characterized by a coupling between the strain and orientational degrees of freedom, whose consequence was

first explored by de Gennes [5]. He showed that, upon the isotropic-nematic transition, homogeneous liquid-crystalline gels should undergo a spontaneous elongation along the director. Later, Golubović and Lubensky [6] showed that homogeneous gels in the nematic phase have soft phonon modes in their ground states. Their model, which is intended for a more general class of non-linear elastic systems, does not explicitly contain the nematic orientational order parameter as a variable. Prior to that, Warner et al. [7] and Abramochuk and Khokhlov [8] independently constructed the first molecular models of nematic networks. Their models are straightforward extensions of the classical theory of rubber elasticity [9], and utilize the fact that nematic polymers, if they are not very rigid, are well described as anisotropic Gaussian chains. The model by Warner et al. is especially general in that it does not assume a certain type of LCP (main-chain or side-chain), and in that it can describe networks crosslinked in the nematic phase as well as those prepared in the isotropic phase. Warner and coworkers [10, 11] have further shown that homogeneous nematic elastomers can be deformed without any change in the elastic free energy, if some special paths of deformation are followed. This effect is called *soft elasticity*. Thermal fluctuations of a homogeneous system have been studied by Olmsted [12] using the same model, in a harmonic approximation.

In this way, the properties of clean and homogeneous nematic gels are now considerably well understood. In experiments, however, a macroscopically homogeneous (or *monodomain*) network is obtained only when a strong magnetic field or a mechanical force is applied in the course of crosslinking, to align the polymers. Networks fabricated without such precaution always contain a large number of director textures. This macroscopically disordered state is called the *polydomain* state. (A *domain* means an orientationally correlated region, and is not necessarily separated from other domains by a sharp interface.) The domain size, or the director correlation length, is typically in the range $10^0 - 10^1$ μm. Polydomain elastomers exhibit unusual non-linear elastic responses against stretching. A typical strain-stress curve starts with a low and almost constant plateau in the small strain region, which is followed by an approximately linear rise of stress in the large strain region [13, 14, 15]. A few recent experiments [16, 17, 18] revealed that the plateau stress can be vanishingly small. The crossover from the soft to hard response roughly corresponds to a change in the state of molecular orientation. In the soft region, the nematic director is inho-

mogeneous and is gradually aligned in the direction of stretching as the strain is increased. In the hard region, the director is almost completely aligned. This crossover in orientation is called the polydomain-monodomain (P-M) transition. To better characterize the state of orientation in the polydomain state, Clarke et al. [19, 15] conducted a polarized light scattering experiment. They obtained an anisotropic scattering intensity with four peaks in the direction of crossed polars, which they call the "four-leaf clover" pattern. Such an anisotropy is not observed in usual fluid nematics with textures.

From theoretical side, the origin of the presumably equilibrium textures has been attributed to some quenched disorder, assumedly introduced by crosslinker molecules [19, 20, 21, 22]. Among them, Fridrikh and Terentjev [21, 22] proposed a random field model which is analogous to models of random anisotropy magnets. They assumed that the external stress linearly couples to the nematic order parameter in the free energy, and tried to explain the stress-orientation relation. On the other hand, little theoretical attention has been paid to neither the stress-strain relation, nor the role of strain-orientation coupling in the polydomain structure.

In this thesis, we study the mechanical response and orientational correlation in nematic gels, with a focus on the long-range elastic interaction between orientational inhomogeneities and quenched sources of randomness. In general, inhomogeneities in an elastic system interacts with each other through an effective long-range interaction mediated by the strain field. The non-local nature of this elastic interaction plays a crucial role in various systems, such as crystalline solids with dislocations and cracks [23], surface adatoms and steps [24], phase separating alloys [25, 26, 27, 28], gels [29], and membranes with inclusions [30]. The present system gives just another example. We assume that the principal source of quenched disorder is provided by the random internal stresses due to heterogeneous chain conformation, and model them on the basis of the affine deformation theory by Warner et al. Then we analyze the long-range elastic interaction. For networks originally prepared in the isotropic phase, we should also take into account the spontaneous deformation induced by the I-N transition. We show that the elastic interaction caused by the spontaneous deformation rearranges the director field in the polydomain state, resulting in the "four-leaf clover" anisotropy in the scattering pattern. This rearrangement realizes a significant reduction of the free energy, which explains the ultra-low

mechanical resistance against stretching. The random stresses act on the order parameter both non-locally and locally, and renders the orientational correlation length finite. We numerically investigate the form of the correlation function, and how the correlation length depends on the strengths of disorder and strain-orientation coupling. We also point out that, if the crosslinking has taken place in the polydomain nematic state, then the initial order parameter acts as a correlated quenched disorder which considerably raises the mechanical stress.

The construction of this thesis is as follows. In the next chapter, we review the notion of random stresses in isotropic gels and extend it to nematic gels. In Chapter 3, first we derive the expression for the elastic interaction, with which we analyze the structure of director and strain fields in the polydomain state. Then we numerically simulate the polydomain state and the polydomain-monodomain transition. We also study the effect of random stresses on soft fluctuations in the monodomain state. We conclude in Chapter 4.

Chapter 2

Model

2.1 Random stresses in isotropic gels

2.1.1 Origins of random stresses

Gels are heterogeneous in nature. One of the main experimental observation that characterizes the heterogeneity in gels is the "abnormal butterfly" pattern obtained by small-angle neutron scattering. Under stretching, the scattering intensity develops bright wings in the direction parallel to stretching. This cannot be understood by assuming the gel to be a homogeneous elastic body. Bastide et al. [31] first pointed out that the crosslink density inhomogeneity can explain the "abnormal" anisotropy direction. Later Onuki [32] proposed a phenomenological continuum model with a random crosslink density, by which he could reproduce the anisotropy tendency. Besides the crosslink density, there can be random anisotropy of the network mesh which is frozen by crosslinking. From the general theory of elasticity, it is known that the free energy of systems bound by central forces can contain a term linear in the metric tensor of deformation. The coefficient of the term may have a spatially inhomogeneous part, which we call the random stress. Alexander [1] pointed out the role of random stresses in systems with small shear rigidity, such as gels and glasses near the glass transition. Shear rigidity of rubbers and gels are typically $10^{-5} - 10^{-6}$ times smaller than that of crystalline solids, and hence they are highly susceptible to internal stresses. However, we cannot know the physical origin of random stresses from these general arguments. Below we discuss the relation between random stresses and the crosslinking conditions of gels.

We consider the classical affine-deformation model of rubber-elasticity [9],

which is derived as follows. A chain whose end-to-end vector is $\boldsymbol{\rho}$ contributes an amount $\ln D(\boldsymbol{\rho})$ to the system's entropy, where

$$D(\boldsymbol{\rho}) = \mathcal{N}^{-1} \exp\left(-\frac{3}{2Na^2}\boldsymbol{\rho}^2\right) \tag{2.1}$$

is the equilibrium probability distribution function of $\boldsymbol{\rho}$. Here N is the polymerization index, a is the size of a monomer, and $\mathcal{N}$ is the normalization factor that assures $\int d\boldsymbol{\rho}\, D(\boldsymbol{\rho}) = 1$. Let us denote the end-to-end vector at the moment of crosslinking by $\boldsymbol{\rho}_0$. State of deformation of the network is described by the deformation gradient tensor,

$$\lambda_{ij} = \frac{\partial r_i}{\partial r_j^0}, \tag{2.2}$$

where $\boldsymbol{r}^0$ and $\boldsymbol{r}$ are the positions of material points at the moment of crosslinking and at observation, respectively. The basic assumption of the model is that, when we apply a macroscopic deformation, the end-to-end vector $\boldsymbol{\rho}_0$ changes to $\boldsymbol{\rho} = \lambda \cdot \boldsymbol{\rho}_0$. Accordingly, the elastic free energy per chain is written as

$$f_{chain} = -k_B T \int d\boldsymbol{\rho}_0 D_0(\boldsymbol{\rho}_0) \ln D(\lambda \quad \boldsymbol{\rho}_0), \tag{2.3}$$

where $D_0(\boldsymbol{\rho}_0)$ is the probability distribution of $\boldsymbol{\rho}_0$. If chains were completely equilibrated at the moment of crosslinking, $D_0(\boldsymbol{\rho}_0) = D(\boldsymbol{\rho}_0)$ and we have

$$f_{chain} = \frac{k_B T}{2} \lambda_{ij} \lambda_{ij} \tag{2.4}$$

(summation over repeated indices i, j, k and l is implied throughout this thesis.) However, crosslinking is a non-equilibrium process that can induce internal flow. Chains in polymer melts are easily deformed by flow and have a large relaxation time due to entanglements. While density fluctuation is suppressed in good solvents, there can remain anisotropic chain deformations at the moment of crosslinking. For small deformations we may assume that the distribution of $\boldsymbol{\rho}_0$ is Gaussian but have an additional weight, as

$$D_0(\boldsymbol{\rho}_0) = \mathcal{N}^{-1} \exp\left(-\frac{3}{2Na^2} \rho_{0,i} A_{ij}^{-1} \rho_{0,j}\right) \tag{2.5}$$

Substituting this into Eq.(2.3), we have $f_{chain} = (k_B T/2)(A_{ij} g_{ij} - \ln \det A)$ where $g_{ij} = \lambda_{ki} \lambda_{kj}$ is the metric tensor. Taking the spatial inhomogeneity of A_{ij} and the crosslink density ν_0 into account, the elastic free energy is obtained as

$$F_{el} = \frac{k_B T}{2} \int d\boldsymbol{r}_0\, \nu_0\, (A_{ij} g_{ij} - \ln \det A) \tag{2.6}$$

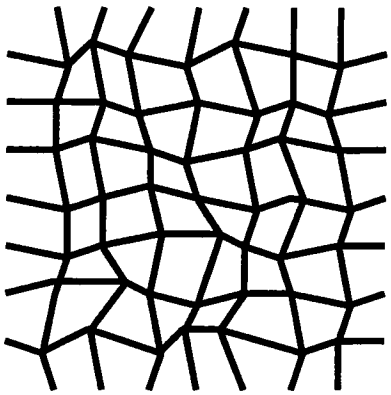

Figure 2.1: Schematic illustration of disordered network structure.

The elastic stress tensor can be computed following a standard procedure [29], and reads

$$\sigma_{ij}^{el} = k_B T \nu_0 A_{kl} \lambda_{ik} \lambda_{jl}. \tag{2.7}$$

In the unperturbed state $\lambda_{ij} = \delta_{ij}$ and in the absence of crosslink density inhomogeneity, its spatial variation is described by the quantity

$$P_{ij} = A_{ij} - \delta_{ij}, \tag{2.8}$$

which we call the (dimensionless) random stress. If we are interested in a length-scale much larger than the the correlation length l_c of the random stress, we can model it as an uncorrelated Gaussian variable. From symmetry, its variance can be written in the form

$$\langle P_{ij}(\boldsymbol{q}) P_{kl}(-\boldsymbol{q}) \rangle = \gamma^2 \left(\delta_{ik}\delta_{jl} + \delta_{il}\delta_{jk} - \frac{2}{d}\delta_{ij}\delta_{kl} \right) + \tilde{\gamma}^2 \, \delta_{ij}\delta_{kl}. \tag{2.9}$$

The quantities γ and $\tilde{\gamma}$ have dimensions of the square root of volume. For instance, if chains at the moment of crosslinking are under shear deformations of magnitude $\sim e$, we have $\gamma \sim l_c^{d/2} e$. Similarly, $\tilde{\gamma}$ describes the magnitude of random chain dilatations. Even if the frozen deformations of individual chains are small, the dimensionless numbers $\nu_0 \gamma^2$ and $\nu_0 \tilde{\gamma}^2$ can be of the order of unity if the deformations are correlated over many chains.

2.1.2 Scattering intensity

To illustrate the role of random stresses, it is useful to see their effect on the butterfly scattering pattern in the neutron scattering intensity. This is done by following Onuki's prescription [32], as follows. The total free energy is written as $F = F_{el} + F_\phi$, where $F_\phi = k_B T \int dr f(\phi)$ is the mixing free energy with ϕ being the volume fraction of polymers. We consider the long-wavelength limit and neglect the gradient free energy. Let us assume $\nu = \overline{\nu} = \text{const}$. For simplicity, we consider only shear random stresses and put $\tilde{\gamma} = 0$. Then the elastic free energy takes the form

$$F_{el} = \frac{k_B T \nu}{2} \int dr \frac{\phi}{\phi_0} \left[g_{ii} + P_{ij} g_{ij} - \ln\left(\frac{\phi}{\phi_0}\right) \right], \tag{2.10}$$

where ϕ_0 is the initial volume fraction and satisfies $\phi_0/\phi = \det \lambda$. The last term is newly included and accounts for an additional entropy due to crosslink distribution over the sample [9]. The deformation can be expressed as $r_i = \overline{\lambda}_{ij} r_{0,j} + u_i$, where $\overline{\lambda}_{ij}$ is the average deformation which is externally controllable, and u_i is the internal displacement and related to the density fluctuation $\delta\phi = \phi - \overline{\phi}$ via $\delta\phi/\overline{\phi} = -\nabla \cdot \boldsymbol{u} + O(|\nabla \boldsymbol{u}|^2)$. The density fluctuation can be written as a sum of two parts; the static fluctuation $\delta\phi_{st}$ and the thermal one, $\delta\phi_{th}$. The former is the solution of the mechanical equilibrium condition, $\nabla \cdot (\sigma^{el} + \sigma^\phi) = 0$, where σ^ϕ is the contribution of F_ϕ to the stress tensor, given by

$$\sigma^\phi_{ij} = k_B T \left(f - \phi \frac{\partial f}{\partial \phi} \right) \delta_{ij}. \tag{2.11}$$

After some calculation, we obtain

$$\delta\phi_{st}(\boldsymbol{q}) = \phi [\epsilon + J_i^2(\hat{\boldsymbol{q}})]^{-1} J_j(\hat{\boldsymbol{q}}) J_k(\hat{\boldsymbol{q}}) P_{jk}(\boldsymbol{q}), \tag{2.12}$$

where

$$\begin{aligned} \hat{\boldsymbol{q}} &= \frac{\boldsymbol{q}}{|\boldsymbol{q}|}, \\ \epsilon &= \theta^{-2} \nu^{-1} \left(1 + \theta^3 \phi^2 \frac{\partial^2 f}{\partial \phi^2} \right), \\ \theta &= \left(\frac{\phi_0}{\phi} \right)^{1/3}, \end{aligned} \tag{2.13}$$

and

$$J_i(\hat{\boldsymbol{q}}) = \theta^{-1} \overline{\lambda}_{ji} \hat{q}_j. \tag{2.14}$$

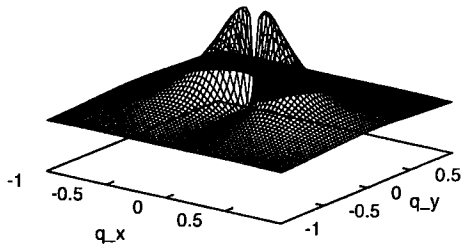

Figure 2.2: Static contribution to the scattering intensity in the presence of shear random stresses and uniaxial stretching. Plotted is Eq.(2.15) with ϵ replaced by $\epsilon + Cq^2$ Parameters are $\lambda_{\|} = 2.0, \lambda_{\perp} = 1.0, \epsilon = 1.0$, and $C = 1.0$.

For isotropic swelling we have $\overline{\lambda}_{ij} = \theta\delta_{ij}$ and $J_i = \hat{q}_i$. The mean square amplitude of the static fluctuation is obtained as

$$I_{st}(\boldsymbol{q}) = \left\langle |\delta\phi_{st}(\boldsymbol{q})|^2 \right\rangle = \phi^2\theta \ \frac{4(\gamma\theta)^2}{3}\left[\frac{J_j^2(\hat{\boldsymbol{q}})}{\epsilon + J_i^2(\hat{\boldsymbol{q}})}\right]^2, \tag{2.15}$$

and that of the thermal fluctuation is given by [32]

$$I_{th}(\boldsymbol{q}) = \left\langle |\delta\phi_{th}(\boldsymbol{q})|^2 \right\rangle = \phi^2\theta \cdot \frac{1}{\nu} \cdot \frac{1}{\epsilon + J_i^2(\hat{\boldsymbol{q}})}. \tag{2.16}$$

As we approach the spinodal line, which is defined by $\inf_{\hat{\boldsymbol{q}}}[\epsilon + J_i^2(\hat{\boldsymbol{q}})] = 0$, the static fluctuation starts to dominate the thermal one. Under uniaxial stretching $\overline{\lambda} = \lambda_{\|}\boldsymbol{e}_x\boldsymbol{e}_x + \lambda_{\perp}(\boldsymbol{e}_y\boldsymbol{e}_y + \boldsymbol{e}_z\boldsymbol{e}_z)$ $(\lambda_{\|} > \lambda_{\perp})$, $I_{th}(\boldsymbol{q})$ develops an anisotropy whose direction is perpendicular to the stretching direction, while $I_{st}(\boldsymbol{q})$ has the opposite ("abnormal") anisotropy. Now we compare $I_{st}(\boldsymbol{q})$ with the static amplitude due to crosslink density inhomogeneity, whose $\hat{\boldsymbol{q}}$-dependence is given as [32]

$$I_{\nu}(\boldsymbol{q}) \propto \left[\frac{J_j^2(\hat{\boldsymbol{q}}) - \theta^{-2}}{\epsilon + J_i^2(\hat{\boldsymbol{q}})}\right]^2 \tag{2.17}$$

The random stresses and the crosslink inhomogeneity give qualitatively similar $\hat{\boldsymbol{q}}$- dependences for a large swelling ratio $\theta \gg 1$, while for $\theta \sim 1$ the results are different. Shown in Fig.2.2 is an example of the abnormal butterfly pattern created by the random stresses.

2.2 Model of disordered nematic gels

2.2.1 Extended affine-deformation theory

The state of order in nematic liquid crystals can be described in terms of the orientational order parameter,

$$Q_{ij} = S\left(n_i n_j - \frac{1}{d}\delta_{ij}\right), \tag{2.18}$$

where S is the scalar order parameter, $\boldsymbol{n}$ is the director, and d is the spatial dimension. Polymers in the nematic phase have anisotropic conformations elongated along the director. To describe the elastic property of nematic networks, Warner, Gelling and Vilgis [7] extended the classical affine-deformation model of rubber elasticity. Their basic assumption is that nematic polymers have anisotropic Gaussian conformations. This is a good approximation if the chain rigidity is not so high and the persistence length is much smaller than the chain contour length. The end-to-end vector distribution in thermal equilibrium is assumed in the form

$$D(\boldsymbol{\rho}) = \mathcal{N}^{-1} \exp\left(-\frac{d}{2Na^2}\rho_i \ell^{-1}_{ij} \rho_j\right), \tag{2.19}$$

where the tensor

$$\ell_{ij} = \ell_{\parallel} n_i n_j + \ell_{\perp}(\delta_{ij} - n_i n_j) \tag{2.20}$$

represents the chain anisotropy. The dimensionless quantities $\ell_{\parallel}$ and $\ell_{\perp}$ depend on the scalar order parameter S. If the crosslinks were introduced in the nematic phase, the chain conformation at that moment is also anisotropic. If the crosslinking took place in equilibrium, the initial distribution is given by

$$D_0(\boldsymbol{\rho}_0) = \mathcal{N}^{-1} \exp\left(-\frac{d}{2Na^2}\rho_{0i} (\ell^0)^{-1}_{ij} \rho_{0j}\right), \tag{2.21}$$

where ℓ^0_{ij} is related to the director $\boldsymbol{n}^0$ at the moment of crosslinking, as

$$\ell^0_{ij} = \ell^0_{\parallel} n^0_i n^0_j + \ell^0_{\perp}(\delta_{ij} - n^0_i n^0_j). \tag{2.22}$$

The elastic free energy is obtained from Eq.(2.3) as

$$F_{el} = \frac{k_B T \nu_0}{2} \int d\boldsymbol{r}_0 \left[\mathrm{Tr}\,(\ell^0 \lambda^T \ell^{-1} \lambda) - \ln \frac{\det \ell^0}{\det \ell}\right] \tag{2.23}$$

The last term in the bracket does not depend on the state of deformation and can be absorbed into the Landau-de Gennes potential for the I-N transition [33], say. Hereafter we neglect this term. We also assume the incompressibility,

$$\det \lambda = 1. \tag{2.24}$$

This is a good approximation for rubbers, and for gels far from the spinodal line. For convenience of analysis, we reparametrize the current and initial conformation tensors in terms of the order parameter, as

$$\ell_{ij}^{-1} = \ell_e^{-1}(\delta_{ij} - \alpha Q_{ij}), \tag{2.25}$$

$$\ell_{ij}^{0} = \ell_e^{0}(\delta_{ij} + \alpha_0 Q_{ij}), \tag{2.26}$$

with

$$\alpha = \frac{1}{S} \frac{\ell_{\parallel} - \ell_{\perp}}{(1-1/d)\ell_{\parallel} + (1/d)\ell_{\perp}}, \tag{2.27}$$

$$\alpha_0 = \frac{1}{S_0} \frac{\ell_{\parallel}^0 - \ell_{\perp}^0}{(1/d)\ell_{\parallel}^0 + (1-1/d)\ell_{\perp}^0}, \tag{2.28}$$

$$\ell_e = \left[\frac{1}{d}\ell_{\parallel}^{-1} + \left(1 - \frac{1}{d}\right)\ell_{\perp}^{-1}\right]^{-1}, \tag{2.29}$$

and

$$\ell_e^0 = \frac{1}{d}\ell_{\parallel}^0 + \left(1 - \frac{1}{d}\right)\ell_{\perp}^0. \tag{2.30}$$

The S- or S_0- dependences of the above four parameters are computed from some microscopic models of LCPs, or obtained from comparison to experiments. However, as they are only weakly dependent on S in typical cases, we shall approximate them by constants. Then we have the basic expression for the free energy of clean incompressible nematic gels as

$$F_{el} = \frac{\mu}{2} \int dr (\delta_{ij} - \alpha Q_{ij})(\delta_{kl} + \alpha_0 Q_{kl}^0)\lambda_{ik}\lambda_{jl}, \tag{2.31}$$

where

$$\mu = k_B T \nu_0 \ell_e^0 \ell_e^{-1} \tag{2.32}$$

is the effective shear modulus. The chain anisotropy is usually large in main-chain LCPs where $\alpha \sim \alpha_0 \sim 1$, while the typical values for side-chain LCPs are $\alpha \sim \alpha_0 \sim 0.1$. Note that α cannot exceed $d/(d-1)$ in the anisotropic limit $\ell_{\parallel}/\ell_{\perp} \to \infty$. Similarly, α_0 is always smaller than d.

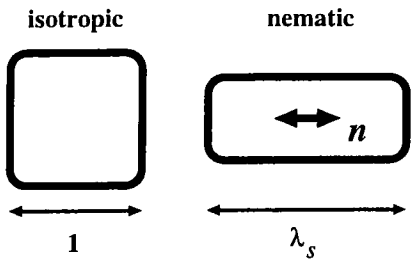

Figure 2.3: If the network is crosslinked in the isotropic phase, a spontaneous elongation along the director is induced by the I-N transition.

Let us look for the homogeneous (monodomain) ground state of this model. Assuming $\boldsymbol{n}^0 = \boldsymbol{e}_x$, $\boldsymbol{n} = \text{const}$, and $\lambda_{ij} = \text{const}$, the minimum of the free energy Eq.(2.31) is located at $\boldsymbol{n} = \boldsymbol{n}_0$ and $\lambda_{ij} = \lambda_s \boldsymbol{e}_x \boldsymbol{e}_x + \lambda_s^{-1/(d-1)} \sum_{a=2}^{d} \boldsymbol{e}_a \boldsymbol{e}_a$, where

$$\lambda_s = \left(\frac{\ell_\parallel}{\ell_\perp} \; \frac{\ell^0_\perp}{\ell^0_\parallel} \right)^{(d-1)/2d} = \left[\frac{1 + (1/d)\alpha S}{1 - (1 - 1/d)\alpha S} \; \frac{1 - (1/d)\alpha_0 S_0}{1 + (1 - 1/d)\alpha_0 S_0} \right]^{(d-1)/2d} \tag{2.33}$$

is the ratio of elongation along the director. If $\ell_{ij} = \ell^0_{ij}$, then $\lambda_s = 1$; no spontaneous deformation will be induced if there is no temperature change.

2.2.2 Random stresses

If we take the non-equilibrium nature of the crosslinking process into account, the initial chain anisotropy tensor ℓ^0_{ij} deviates from that given by Eq.(2.26), as

$$\ell^0_{ij} = \ell^0_e(\delta_{ij} + \alpha_0 Q_{ij} + P_{ij}), \tag{2.34}$$

where P_{ij} is the non-equilibrium contribution, which we shall refer to as the random stress. Now we arrive at the most general form of the elastic free energy we shall utilize,

$$F_{el} = \frac{\mu}{2} \int dr (\delta_{ij} - \alpha Q_{ij})(\delta_{kl} + \alpha_0 Q^0_{kl} + P_{kl}) \lambda_{ik} \lambda_{jl}. \tag{2.35}$$

However, full treatment of this model is too complex and not very fruitful. In Sections 3.1-3.3 below, we shall consider the following two essential cases.

Case I. (crosslinking in the isotropic phase)
The network is obtained by crosslinking a polymer melt in the isotropic phase

($\alpha_0 = 0$) and a subsequent quench into the nematic phase. The source of quenched disorder is the random stress P_{ij}, which is a Gaussian variable obeying Eq.(2.9). We further assume that the chain dilatation is homogeneous, or $\gamma' = 0$, and there are only shear random stresses. Although it is not fully justified, we may point out that the density fluctuation is strongly suppressed in dense polymer melts, while an internal shear flow can easily deform chains. The material is characterized by two parameters, α and γ.

Case II. (crosslinking in the nematic phase)
Nematic polymer melts often exhibit long-lived polydomain textures, which coarsen very slowly [40]. In some experiments [17], polydomain elastomers are obtained by crosslinking a polydomain melt in the nematic phase. Let us assume that the crosslinking occurred at one moment during the phase ordering kinetics after a quench from the isotropic phase, and that the temperature is unchanged since then. In this case we have $\alpha_0 = \alpha/[1-(1-2/d)\alpha]$ from $\ell_{||}^0 = \ell_{||}$ and $\ell_{\perp}^0 = \ell_{\perp}$. We assume that the initial chains have been equilibrated, or $P_{ij} = 0$. The orientational configuration of the original melt is memorized into the network, and acts as the source of quenched disorder. The effective disorder strength depends on the correlation length ξ_0 of the initial configuration Q_{ij}^0. The basic material parameters are thus α and ξ_0.

Chapter 3

Analysis of elastic effects

3.1 Elastic interactions

The quenched inhomogeneities P_{ij} and Q^0_{ij} produce heterogeneous deformations at mechanical equilibrium. A local source of disorder creates a long-range strain field around it and affects the nematic order parameter Q_{ij} in remote places. The order parameter field interacts also with itself, mediated by the strain field. In this section, we derive the explicit forms of these elastic interactions, to prepare for discussion of director correlation and mechanical responses in the following sections. Throughout the chapter, we shall regard the average strain $\overline{\lambda}_{ij}$ as an externally controlled parameter. We also assume that the external deformation is a uniaxial stretching in the x-direction, written as

$$\overline{\lambda} = \lambda_{\parallel} e_x e_x + \lambda_{\perp} \sum_{a=2}^{d} e_a e_a, \quad \lambda_{\perp} = \lambda_{\parallel}^{-1/(d-1)}. \tag{3.1}$$

3.1.1 Harmonic approximation

Expansion in internal strain

First we consider the case with no average deformation ($\overline{\lambda}_{ij} = \delta_{ij}$). The elastic free energy can be expanded with respect to the internal strain $\nabla \boldsymbol{u}$ where $\boldsymbol{u} = \boldsymbol{r} - \boldsymbol{r}_0$ is the internal displacement. Substituting $\lambda_{ij} = \delta_{ij} + \partial_j u_i$ into Eq.(2.35), we have

$$\begin{aligned} F_{el} &= \frac{d}{2}\mu + \Delta F_{el}, \\ \Delta F_{el} &= \frac{\mu}{2} \int d\boldsymbol{r} \Big[(\partial_i u_j)^2 - 2(\alpha Q_{ij} - P_{ij}) \partial_i u_j - \alpha Q_{ij} P_{ij} + K (\partial_i u_i)^2 \Big] \end{aligned} \tag{3.2}$$

in a harmonic approximation. The final term in the integrand is added to temporarily relax the incompressibility $\nabla \ \boldsymbol{u} = 0$, which will be recovered by taking the limit $K \to \infty$ at the end of calculation.

To discuss static properties, we can eliminate the strain field using the mechanical equilibrium condition,

$$\frac{\delta F}{\delta \boldsymbol{u}} = 0, \tag{3.3}$$

which gives a functional of Q_{ij} only. The harmonic approximation is valid if the quenched disorder is weak and if the strain-orientation coupling is small, or,

$$\alpha S \ll 1. \tag{3.4}$$

The former condition is written in terms of the lower-cutoff length b of the coarse-graining. The strain $\nabla \boldsymbol{u}$ at the coarse-grained level is small if

$$\gamma \, b^{-d/2} \ll 1. \tag{3.5}$$

The latter condition Eq.(3.4) is satisfied in the following cases; (i) $S \ll 1$: pretransitional fluctuation. (ii) $\alpha \ll 1$, $S \sim 1$: nematic phase with weak coupling.

Weak disorder limit

In the absence of random stresses, Eq.(3.2) becomes

$$\Delta F_{el} \ = \ \frac{\mu}{2} \int d\boldsymbol{r} \Big[(\partial_i u_j)^2 - 2\alpha Q_{ij} \partial_i u_j + K (\partial_i u_i)^2 \Big], \tag{3.6}$$

from which the mechanical equilibrium condition Eq.(3.3) reads

$$-K \partial_i \partial_j u_j - \nabla^2 u_i + \alpha \partial_j Q_{ij} \ = \ 0. \tag{3.7}$$

From its Fourier transform,

$$K q_i q_j u_j(\boldsymbol{q}) + q^2 u_i(\boldsymbol{q}) + \sqrt{-1} \, \alpha \, q_j Q_{ij}(\boldsymbol{q}) \ = \ 0, \tag{3.8}$$

we have

$$u_i(\boldsymbol{q}) = \frac{-\sqrt{-1} \, \alpha}{q^2} \left[q_j Q_{ij}(\boldsymbol{q}) - \frac{K}{K+1} \frac{q_i q_j}{q^2} q_k Q_{jk}(\boldsymbol{q}) \right] \tag{3.9}$$

In the incompressible limit $K \to \infty$, it becomes

$$u_i = \frac{\alpha}{\nabla^2} \left(\delta_{ij} - \frac{\partial_i \partial_j}{\nabla^2} \right) \partial_k Q_{jk}, \tag{3.10}$$

which is substituted back to Eq.(3.6) to yield

$$\begin{aligned}\Delta F_{el} &= -\frac{\mu\alpha^2}{2}\int dr\left[\left(\frac{1}{\nabla^2}\partial_i\partial_j Q_{ij}\right)^2-\left(\frac{1}{\nabla^2}\partial_i\partial_k Q_{jk}\right)^2\right] \\ &= -\frac{\mu\alpha^2}{2}\int_{\boldsymbol{q}}\left[\left|\hat{q}_i\hat{q}_j Q_{ij}(\boldsymbol{q})\right|^2-\left|\hat{q}_i\hat{q}_k Q_{jk}(\boldsymbol{q})\right|^2\right], \qquad (3.11)\end{aligned}$$

where $\hat{q}_i = q_i/|\boldsymbol{q}|$ and $\int_{\boldsymbol{q}} = \int(2\pi)^{-d}d\boldsymbol{q}$.

Hereafter we consider the two-dimensional case. In 2D, the traceless symmetric tensor Q_{ij} has only two independent components, say Q_{xx} and Q_{xy}. This makes the analytical treatment particularly simple. Eq.(3.11) can be rewritten as

$$\Delta F_{el} = -\frac{\mu\alpha^2}{2}\int_{\boldsymbol{q}}|Q_1(\boldsymbol{q})|^2, \qquad (3.12)$$

where

$$\begin{aligned}Q_1(\boldsymbol{q}) &= 2\hat{q}_x\hat{q}_y Q_{xx}(\boldsymbol{q})-(\hat{q}_x^2-\hat{q}_y^2)Q_{xy}(\boldsymbol{q}) \\ &= \sin 2\varphi\; Q_{xx}(\boldsymbol{q})-\cos 2\varphi\; Q_{xy}(\boldsymbol{q}). \qquad (3.13)\end{aligned}$$

We have introduced the azimuthal angle φ of the wavevector $\boldsymbol{q} = |\boldsymbol{q}|(\cos\varphi, \sin\varphi)$. A complementary variable can be defined by

$$\begin{aligned}Q_2(\boldsymbol{q}) &= (\hat{q}_x^2-\hat{q}_y^2)Q_{xx}(\boldsymbol{q})+2\hat{q}_x\hat{q}_y Q_{xy}(\boldsymbol{q}) \\ &= \cos 2\varphi\; Q_{xx}(\boldsymbol{q})+\sin 2\varphi\; Q_{xy}(\boldsymbol{q}). \qquad (3.14)\end{aligned}$$

Note that $Q_1(\boldsymbol{q})$ and $Q_2(\boldsymbol{q})$ constitute a set of normal modes and satisfy

$$|Q_1(\boldsymbol{q})|^2+|Q_2(\boldsymbol{q})|^2 = |Q_{xx}(\boldsymbol{q})|^2+|Q_{xy}(\boldsymbol{q})|^2 \qquad (3.15)$$

The inverse Fourier transform of $Q_a(\boldsymbol{q})$ $(a = 1, 2)$ will be denoted by $Q_a(\boldsymbol{r})$, which are real variables.

Effect of quenched disorder

The effect of random stresses on the long-range interaction can be included by replacing αQ_{ij} by $\alpha Q_{ij} - P_{ij}$ in Eq.(3.11) (see Eq.(3.2)). The effective free energy in 2D now reads

$$\Delta F_{el} = -\frac{\mu}{2}\int_{\boldsymbol{q}}\Big[\Big|\alpha Q_1(\boldsymbol{q})-P_1(\boldsymbol{q})\Big|^2+\alpha Q_{ij}(\boldsymbol{q})P_{ij}(-\boldsymbol{q})\Big]. \qquad (3.16)$$

where $P_1(\boldsymbol{q})$ is defined by an equation parallel to Eq.(3.13). Note that the quenched disorder both locally and non-locally acts on the order parameter. If we incorporate the dilatational part of random stresses, P_{ij} in the above formula should be replaced by its shear part $P_{ij}^S = P_{ij} - (1/d)P_{kk}\delta_{ij}$, and P_1 by P_1^S The bulk part $(1/d)P_{kk}\delta_{ij}$ does not affect the order parameter, at least in the harmonic approximation and in the unstretched case.

Effect of stretching

The effect of external stretching can be incorporated by expanding Eq.(2.35) with respect to the internal displacement, which is redefined as $\boldsymbol{u} = \boldsymbol{r} - \overline{\lambda}\ \ \boldsymbol{r}_0$. In the absence of quenched disorder, the effective free energy is obtained as

$$\begin{aligned} F_{el} &= \text{const.} - \mu\alpha \int d\boldsymbol{r}\ (\overline{W} - I) : Q(\boldsymbol{r}) \\ &- \frac{\mu\alpha^2}{2} \int_{\boldsymbol{q}} \frac{1}{\overline{\overline{W}} : \hat{\boldsymbol{q}}\hat{\boldsymbol{q}}} \left[\left| (\overline{W} \cdot \hat{\boldsymbol{q}}) \cdot Q(\boldsymbol{q}) \right|^2 - \left| (\overline{W} \cdot \hat{\boldsymbol{q}}) \cdot Q(\boldsymbol{q}) \cdot \hat{\boldsymbol{q}} \right|^2 \right], \quad (3.17) \end{aligned}$$

where $\overline{W}_{ij} = \overline{\lambda}_{ik}\overline{\lambda}_{jk}$. The first integral in the right hand side has a tendency to align the director in the direction of stretching, while the long-range interaction represented by the second integral acts against it.

Nonlinear effect

Now we briefly comment on nonlinear effects. Including the next higher (third) order terms into Eq.(3.6), we have

$$\begin{aligned} \Delta F_{el} &= \frac{\mu}{2} \int d\boldsymbol{r} \Big\{ (\partial_i u_j)^2 - 2\alpha Q_{ij}\partial_i u_j - \alpha Q_{ij}(\partial_k u_i)(\partial_k u_j) \\ &\qquad + K \Big[(\partial_i u_i)^2 + (\partial_i u_i)^3 - (\partial_i u_i)(\partial_j u_k)(\partial_k u_j) \Big] \Big\}. \quad (3.18) \end{aligned}$$

The final term is derived from $K(\det\lambda - 1)^2$, using the expansion

$$\det\lambda - 1 = \partial_i u_i + (1/2)[(\partial_i u_i)^2 - (\partial_i u_j)(\partial_j u_i)] + O(|\nabla \boldsymbol{u}|^3). \quad (3.19)$$

Following a standard procedure of perturbation expansion, we can obtain the third order contribution to the effective free energy, written in terms of three-body long-range interactions. More generally, we have n-body non-local interactions in the n-th order. This is different from the case of elastic systems coupled with a scalar order parameter, where we have a two-body interaction in the third order [28]. Unfortunately, we find no realistic situation whether a further

analysis of the three-body interactions is both useful and tractable. Although a next higher order calculation may serve to specify the bifurcation class of the director buckling instability (cf. Section 3.4), we abandon any nonlinear analysis in this thesis.

3.1.2 Pretransitional behavior

The role of elastic interactions can be illustrated by considering thermal fluctuation of the order parameter above the isotropic-nematic transition. The I-N transition is a weakly first order transition and the correlation length just above the transition is typically of the order of tens of nanometers. Pretransitional fluctuation in nematic fluids has been extensively studied by light scattering and electric or magnetic birefringences, although there is yet little study for nematic networks.

The total free energy can be written as $F = F_{el} + F_L$, where F_L is the Landau-de Gennes potential in the harmonic approximation,

$$F_L = \int d\boldsymbol{r} \left[\frac{A}{2} \mathrm{Tr}\, Q^2 + \frac{L_1}{2} (\partial_i Q_{jk})^2 + \frac{L_2}{2} (\partial_i Q_{ij})^2 \right], \tag{3.20}$$

where $A = a(T - T_*)$. In 2D we obtain

$$\begin{aligned} F &= \frac{1}{2} \int_{\boldsymbol{q}} \left[\left(A - \mu\alpha^2 + Lq^2 \right) |Q_1(\boldsymbol{q})|^2 + \left(A + Lq^2 \right) |Q_2(\boldsymbol{q})|^2 \right], \\ L &= L_1 + \frac{L_2}{2}, \end{aligned} \tag{3.21}$$

using Eqs.(3.12) and (3.15). From this we see that the spinodal temperature is shifted from T_* to $T_* - \mu\alpha^2/a$, which is the result obtained long ago by de Gennes [5] assuming spatial homogeneity. Let us consider the depolarized scattering intensity. When one of the polars lies in the x-direction and another in the y-direction, the scattering intensity is given by

$$I(\boldsymbol{q}) = \left\langle |Q_{xy}(\boldsymbol{q})|^2 \right\rangle, \tag{3.22}$$

except for a wave-vector independent prefactor [33]. From Eq.(3.21) we have

$$\begin{aligned} I(\boldsymbol{q}) &= \cos(2\varphi)^2 \left\langle |Q_1(\boldsymbol{q})|^2 \right\rangle + \sin(2\varphi)^2 \left\langle |Q_2(\boldsymbol{q})|^2 \right\rangle \\ &= \cos(2\varphi)^2 \frac{k_B T}{A - \mu\alpha^2 + Lq^2} + \sin(2\varphi)^2 \frac{k_B T}{A + Lq^2}. \end{aligned} \tag{3.23}$$

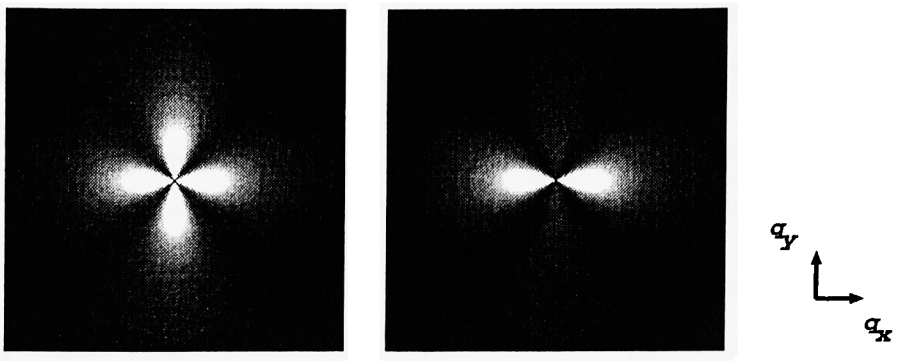

Figure 3.1: Depolarized scattering intensity above the I-N transition. The temperature is $T = T_* - 0.9\mu\alpha^2/a$. Left : without stretching. Right : with stretching in the x-direction ($\lambda_{\|} = 1.2$, $\alpha = 1$).

At a temperature slightly above the spinodal, there arises a strong asymmetry $\langle|Q_1(\boldsymbol{q})|^2\rangle \gg \langle|Q_2(\boldsymbol{q})|^2\rangle$ and the scattering intensity becomes largest at $\varphi = n\pi/2$ (n: integer), and exhibits a "four-leaf clover"-shaped pattern as shown in Fig.3.1. At short wavelengths the anisotropy is diminished by the Frank elasticity. The balance between rubber elasticity and Frank elasticity defines a characteristic length,

$$\xi_c = \sqrt{\frac{L}{\mu\alpha^2}}. \tag{3.24}$$

A typical set of experimental values $L \sim 10^{-11}N$, $\mu \sim 10^5 J/m^3$, and $\alpha \sim 1$ gives $\xi_c \sim 10^1 nm$ as a rough estimate.

The effect of stretching can be readily incorporated in the above calculation. The depolarized scattering intensity, which is obtained from Eq.(3.17), is more enhanced in the direction of stretching, as shown in Fig.3.1. However, there is a reservation in use of the harmonic approximation. The free energy density responsible for this stretching-induced anisotropy is of the order of $\mu(\lambda_{\|}-1)(\alpha S)^2$, as seen from Eq.(3.17) (Note that the first integral in the r.h.s of Eq.(3.17) is not relevant for fluctuation at finite wavenumbers.) On the other hand, terms of the order of $\mu(\alpha S)^3$ appear in the third order expansion of the free energy. Therefore, the calculation based on the harmonic approximation is well justified only if $\lambda_{\|} - 1 \gg \alpha S$.

3.2 Polydomain State

The harmonic approximation in the previous section is valid also in the nematic phase with $S \sim 1$, if the coupling α is much smaller than unity. For simplicity's sake, we put $S = 1$ hereafter. The free energy in the nematic phase is written as the sum of the elastic and the Frank free energy, the latter being

$$F_F = \int dr \frac{K_F}{2} (\partial_i n_j)^2 \tag{3.25}$$

in the one-constant approximation [33]. The characteristic length ξ_c is now redefined by

$$\xi_c = \sqrt{\frac{K_F}{\mu\alpha^2}}. \tag{3.26}$$

Since L and K_F are of the same order, we again have $\xi_c \alpha \sim 10\ nm$, and $\xi_c \sim 10^2\ nm$ for a weak coupling $\alpha \sim 0.1$. The polydomain state is characterized by two lengths, ξ_c and the director correlation length which we denote by ξ. In typical experiments $\xi \sim 1 - 10\ \mu m$, and hence there is a sizable gap between ξ_c and ξ, where the elastic interaction of the order parameter plays an important role.

3.2.1 Weak disorder limit

First we assume the quenched disorder to be sufficiently weak and neglect it.

Real space correlation

Eq.(3.11) can be rewritten in the form

$$\begin{aligned} \Delta F_{el} &= -\frac{\mu\alpha^2}{2} \int dr \int dr' \Big[Q_{ik}(r)\ \partial_i \partial_j G_2(r - r') \cdot Q_{jk}(r) \\ &\qquad + Q_{ij}(r) \cdot \partial_i \partial_j \partial_k \partial_l G_4(r - r') \cdot Q_{kl}(r') \Big], \end{aligned} \tag{3.27}$$

where $G_n(r)$ $(n = 2, 4)$ are the Green functions defined by

$$\nabla^n G_n(r) = -\delta(r), \tag{3.28}$$

$$G_n(r \to \infty) = 0. \tag{3.29}$$

In 2D, Eq.(3.27) can be reduced into the form

$$\Delta F_{el} = \frac{\mu\alpha^2}{16\pi} \int dr \int dr' \frac{1}{R^2} \cos[2(\theta - \varphi_R) + 2(\theta' - \varphi_R)], \tag{3.30}$$

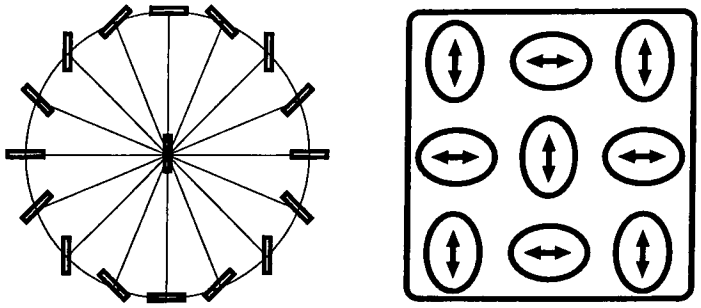

Figure 3.2: Left : preferred director configuration in 2D. The director at the center is fixed, and the optimal directors at surrounding points are plotted. Right : Ellipses indicate the anisotropy of local strain.

where $\boldsymbol{R} = \boldsymbol{r} - \boldsymbol{r}'$, and θ, θ', φ_R are the azimuthal angles of $\boldsymbol{n}(\boldsymbol{r})$, $\boldsymbol{n}(\boldsymbol{r}')$, and $\boldsymbol{R}$, respectively. This free energy prefers the relative director orientation that satisfies

$$(\theta - \varphi_R) + (\theta' - \varphi_R) = \left(n + \frac{1}{2}\right)\pi \qquad (n : \text{integer}), \tag{3.31}$$

which is depicted in Fig.3.2. When the local director points to the north (and south), the correlation is enhanced in the northeast, northwest, southeast and southwest directions and suppressed in the north, south, east and west directions. This has a following simple interpretation : the center region is elongated along the director and pushes the north and south neighbor regions, which will elongate into east and west directions to reduce the conflict. Thus the director vectors in the north and south tend to be perpendicular to the central one. In contrast, the regions in the east and west neighborhoods are pulled toward the center, which also leads to the perpendicular orientation.

In 3D, the free energy Eq.(3.27) becomes

$$\Delta F_{el} = \frac{\mu\alpha^2}{16\pi}\int d\boldsymbol{r}\int d\boldsymbol{r}'\frac{1}{R^3}\, g(\boldsymbol{n},\boldsymbol{n}',\hat{\boldsymbol{R}}), \tag{3.32}$$

$$\begin{aligned} g(\boldsymbol{n},\boldsymbol{n}',\hat{\boldsymbol{R}}) &= -\frac{5}{3} + 4(\boldsymbol{n}\cdot\boldsymbol{n}')^2 + (\boldsymbol{n}\cdot\hat{\boldsymbol{R}})^2 + (\boldsymbol{n}'\ \hat{\boldsymbol{R}})^2 \\ &- 18(\boldsymbol{n}\cdot\boldsymbol{n}')(\boldsymbol{n}\cdot\hat{\boldsymbol{R}})(\boldsymbol{n}'\ \hat{\boldsymbol{R}}) + 15(\boldsymbol{n}\ \hat{\boldsymbol{R}})^2(\boldsymbol{n}'\ \hat{\boldsymbol{R}})^2, \end{aligned} \tag{3.33}$$

where $\hat{\boldsymbol{R}} = \boldsymbol{R}/|\boldsymbol{R}|$. Correlation in directions parallel and perpendicular to the director is suppressed as in the 2D case, which is known by observing that the

function

$$g(\boldsymbol{n}, \boldsymbol{n}', \boldsymbol{n}) = -\frac{2}{3} + 2(\boldsymbol{n} \cdot \boldsymbol{n}')^2 \tag{3.34}$$

takes the minimum when $\boldsymbol{n} \perp \boldsymbol{n}'$

Soft response

Next we compute the elastic free energy in the 2D case. As in the pretransitional case, an asymmetry $|Q_1(\boldsymbol{q})|^2 > |Q_2(\boldsymbol{q})|^2$ arises to reduce the elastic free energy Eq.(3.12). Because of Eq.(3.15), we have

$$\overline{Q_1(\boldsymbol{r})^2} + \overline{Q_2(\boldsymbol{r})^2} = \overline{Q_{xx}(\boldsymbol{r})^2} + \overline{Q_{yy}(\boldsymbol{r})^2} = \frac{1}{4}. \tag{3.35}$$

We expect to have

$$\overline{Q_1(\boldsymbol{r})^2} = \frac{1}{4}, \qquad \overline{Q_2(\boldsymbol{r})^2} = 0. \tag{3.36}$$

Although it is difficult to prove Eq.(3.36) because of the local constraint $Q_{xx}(\boldsymbol{r})^2 + Q_{xy}(\boldsymbol{r})^2 = 1/4$, we have confirmed it by numerical simulation (cf. Section 3.3). The elastic free energy density (averaged over the space) is given by

$$\Delta f_{el} = -\frac{\mu\alpha^2}{2}\overline{Q_1(\boldsymbol{r})^2} = \frac{\mu\alpha^2}{8} \tag{3.37}$$

Now it can be shown that, in the weak disorder limit, the P-M transition accompanies only a small change of $O(\alpha^3)$ in the elastic free energy. Indeed, the elastic free energy density at the monodomain state with $\lambda = \lambda_s$ is obtained from Eqs.(2.31) and (2.33) as

$$f_{el,mono} = \mu\sqrt{1 - \frac{\alpha^2}{4}}, \tag{3.38}$$

which is equal to $f_{el} = \mu + \Delta f_{el}$ to order α^2. In order to understand the origin of this soft response, it is useful to look at the local stress in the polydomain state. The elastic stress tensor is obtained from Eq.(3.6) as

$$\sigma_{ij} = \mu(\partial_i u_j + \partial_j u_i - \alpha Q_{ij}). \tag{3.39}$$

Substituting Eq.(3.9), we obtain its variance as

$$\overline{\sigma_{ij}(\boldsymbol{r})^2} = \mu^2\alpha^2\overline{Q_2(\boldsymbol{r})^2} = 0, \tag{3.40}$$

which means that each part of the system is elongated along the local director by $1 + \alpha/4 = \lambda_s + O(\alpha^2)$ times.

Scattering intensity

Using the anomalous diffraction approximation, Clarke et al. [19] showed that the wave-vector dependence of the depolarized scattering intensity in the polydomain state is again given by $I(\boldsymbol{q}) = \langle |Q_{xy}(\boldsymbol{q})|^2 \rangle$, if the director lies in the x-y plane. Then the asymmetry $|Q_1(\boldsymbol{q})|^2 > |Q_2(\boldsymbol{q})|^2$ leads the "four-leaf clover" type anisotropy, although the explicit form of $I(\boldsymbol{q})$ can not be calculated.

3.2.2 Effect of quenched disorder

The effects of quenched random fields on systems with a continuous symmetry have previously been studied in terms of many different physical systems, such as random anisotropy magnets [34], vortex lattices in superconductors, charge-density-waves, and nematic fluids in porous media [35]. In an earliest study, Imry and Ma [36] showed that a long-range orientational order in dimensions lower than four is destroyed by an arbitrary weak random field. Let us recapitulate their argument using the free energy

$$F_{rf} = \int dr \left[\frac{K_F}{2} (\nabla \boldsymbol{n})^2 - (\boldsymbol{H} \cdot \boldsymbol{n})^2 \right], \tag{3.41}$$

where $\boldsymbol{H}$ is a field with a constant magnitude H_0 and with random directions whose correlation decays in a distance b. It is convenient to descretize the space into a lattice with a grid size b and the rewrite Eq.(3.41) in the form

$$F_{rf} = \sum_{\langle ss' \rangle} \frac{k_F}{2} (\boldsymbol{n}_s - \boldsymbol{n}_{s'})^2 - \sum_s (\boldsymbol{h}_s \cdot \boldsymbol{n}_s)^2, \tag{3.42}$$

where $k_F \sim K_F b^{d-2}$, $|\boldsymbol{h}_s| = h_0 \sim H_0 b^{d/2}$, and $\boldsymbol{h}_s$ is randomly oriented from site to site. Consider a polydomain state with a correlation length ξ much larger than b. Each domain contains typically $N = (\xi/b)^d$ sites. By choosing an optimal director orientation, a domain can reduce its random field energy by around $\sqrt{N} h_0^2$, while it obtains gradient free energy $\sim N k_F/(\xi/b)^2$. Equating these two contributions, we have

$$\left(\frac{\xi}{b} \right)^{2-d/2} \sim \frac{k_F}{h_0^2} \sim \frac{K_F}{H_0^2 b^2}. \tag{3.43}$$

For $d < 4$, ξ is finite and has a power-law dependence on the random field strength, which is the original finding by Imry and Ma. Note that, in their estimate of the disorder free energy, the random field is assumed to be a weak

perturbation to a uniformly aligned director field, and the feedback due to the change of director is not considered. They also neglected the effect of vortices (disclinations), around which the director drastically changes its orientation.

Correlation in the random-field 2D XY model, defined by a Hamiltonian equivalent to Eq.(3.42), has been studied by Monte Carlo simulations [37, 38]. Gingras and Huse [37] performed a simulation at finite temperature (below the critical temperature of the non-disordered XY model), and found that the correlation function $G(r) = \left\langle (\boldsymbol{n}(0)\cdot\boldsymbol{n}(\boldsymbol{r}))^2 - \frac{1}{2} \right\rangle$ decays slightly faster than an exponential function. With the same model but at $T = 0$, Yu et.al. [38] found that $-\ln(\xi/b)$ is approximately proportional to the effective disorder strength $D = h_0^2/k_F$, and that $G(r)$ is well fitted by a simple exponential function for a large value of D (that gives $\xi/b \sim 1$). With a slightly different Hamiltonian (equivalent to Eq.(3.42) except for lacking the $\boldsymbol{n} \leftrightarrow -\boldsymbol{n}$ symmetry) and at $T = 0$, Dieny and Barbara [39] also found that $G(r)$ decays a little faster than an exponential function and that $-\ln(\xi/b)$ is proportional to D.

3.2.3 Crosslinking in the nematic phase

Elastic interactions in the Case II is obtained by simply replacing P_{ij} in Eq.(3.16) by αQ^0_{ij} (note that $\alpha_0 = \alpha$ in 2D). There are two qualitatively different behaviors depending on the orientational correlation length ξ_0 at the moment of crosslinking.

Case II-A : $\xi_0 \lesssim \xi_c$
If the crosslinking has taken place at an early stage of the phase ordering, Q^0_{ij} has a microscopic correlation length and so its qualitative role is same to that of P_{ij}. Domains will continue to grow to reduce the Frank free energy until finally pinned by the random field.

Case II-B : $\xi_0 \gtrsim \xi_c$
If domains have already grown to macroscopic sizes when the crosslinks are introduced, Q^0_{ij} acts as a correlated disorder and strongly pins the directure texture. We expect to have $Q_{ij}(\boldsymbol{r}) \simeq Q^0_{ij}(\boldsymbol{r})$ at equilibrium.

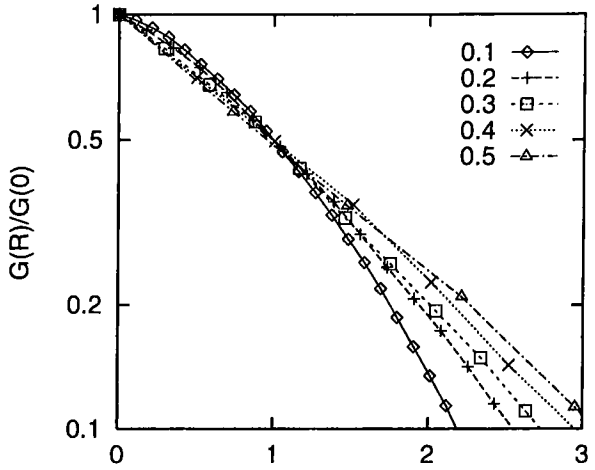

Figure 3.3: Director correlation function $G(R)/G(0)$ for the effective disorder strength $D = 0.1, 0.2, 0.3, 0.4, 0.5$. The horizontal axis is the scaled distance R/ξ. Fixed parameters are $\alpha = 0.1$ and $\mu = 200$.

3.2.4 Effect of stretching

Here we remark on the effect of stretching on the director correlation. As mentioned in the previous section, the harmonic approximation Eq.(3.11) can tell the correct anisotropy only if $\lambda_{\|} - 1 \gg \alpha S (= \alpha)$. Unfortunately, this condition is satisfied only in the monodomain state. In order to study the effect of stretching on the correlation function in the polydomain state, we have to resort to direct numerical simulation of the non-linear model Eq.(2.35).

3.2.5 Numerical Simulation

To study orientational correlation in the polydomain state, we have conducted a numerical simulation in two spatial dimensions. As the dynamics is glassy due to the quenched randomness, we used an annealing method to facilitate numerical minimization of the free energy. We solved the Langevin equation for the director,

$$\frac{\partial \boldsymbol{n}}{\partial t} = \Big(I - \boldsymbol{n}\boldsymbol{n}\Big) \ \Big(-\Gamma_{\boldsymbol{n}} \frac{\delta F}{\delta \boldsymbol{n}} + \boldsymbol{\eta}_{\boldsymbol{n}}\Big), \tag{3.44}$$

where $\boldsymbol{\eta}_{\boldsymbol{n}}$ is an uncorrelated Gaussian thermal noise. Its mean square amplitude was gradually reduced and finally turned off to reach the free energy minimum. We assumed a weak coupling and utilized the harmonic elastic free energy

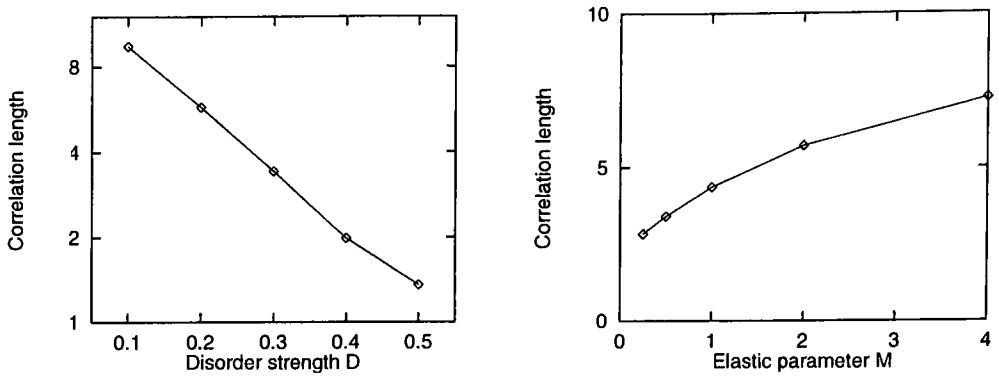

Figure 3.4: Left : Correlation length as a function of D, with $M = 0.5$ fixed. Right : Correlation length as a function of M, with $D = 0.3$ fixed.

Eq.(3.2), so that the internal displacement can be determined by solving linear equation Eq.(3.8) by Fast Fourier Transform. The periodic boundary condition was imposed on both $\boldsymbol{u}$ and $\boldsymbol{n}$. The grid size b was taken to be unity. A standard set of parameters used was $K_F = 4, \mu = 200, \alpha = 0.1$, and $\gamma = 0.06$, for which the characteristic length ξ_c equals 1.4. The effective strength of disorder is described by the dimensionless parameter,

$$D = \frac{\mu\alpha\gamma}{K_F} \cdot b. \tag{3.45}$$

The strength of rubber-elastic effect in comparison with Frank elasticity is described by

$$M = \frac{\mu\alpha^2}{K_F} \cdot b^2 = \left(\frac{b}{\xi_c}\right)^2 \tag{3.46}$$

Average over 20 independent samples were taken for each set of parameters to obtain the correlation function.

First consider the ordinary correlation function,

$$G(|\boldsymbol{R}|) \;=\; \Big\langle Q_{ij}(\boldsymbol{r}) Q_{ij}(\boldsymbol{r}+\boldsymbol{R}) \Big\rangle. \tag{3.47}$$

We defined the correlation length ξ by

$$\frac{G(\xi)}{G(0)} = \frac{1}{e} \tag{3.48}$$

The numerical data are shown in Fig.3.3. The decay of $G(R)$ is nearly exponential for a strong disorder and faster for a weaker disorder. This qualitative

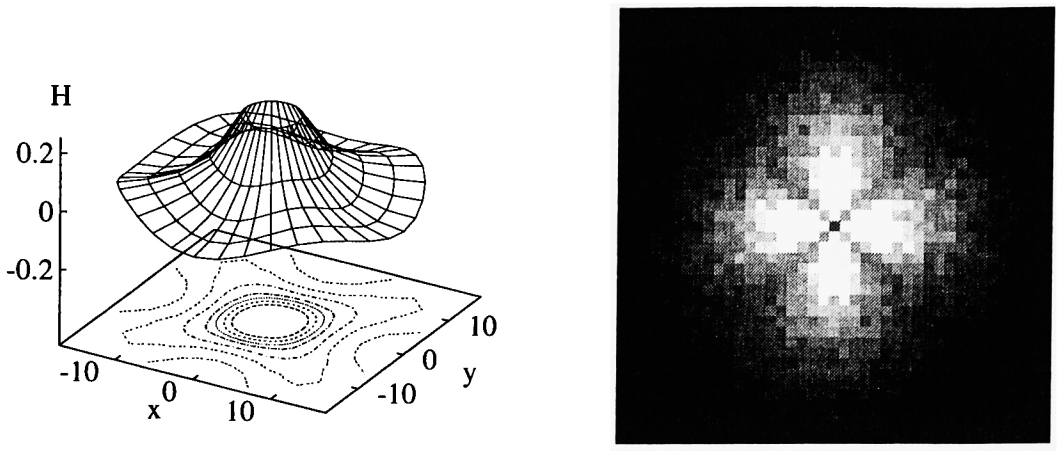

Figure 3.5: Left : Director-relative correlation function $H(\boldsymbol{R})$. Plotted range is $R \geq \xi$. Right : Depolarized light scattering intensity $I(\mathbf{q}) = \langle |Q_{xy}(\mathbf{q})|^2 \rangle$.

tendency agrees with previous results for the 2D random-field XY model [37, 38]. The correlation length ξ strongly depends on the effective disorder strength D, as shown in Fig.3.4. The dependence is roughly exponential, also in agreement with previous results [38, 39] for the XY model. In the same figure we show the dependence of ξ on the parameter M, which is not strong; the correlation length is basically determined by a balance between Frank elasticity and the effect of quenched disorder.

To quantify the director-relative correlation featured in Fig.3.2, we also computed the function

$$\begin{aligned} H(\boldsymbol{R}) &= \Big\langle Q_{ij}(\boldsymbol{r}) Q_{ij}(\boldsymbol{r} + U \ \ \boldsymbol{R}) \Big\rangle, \\ U(\boldsymbol{r}) &= \begin{bmatrix} \cos\theta & -\sin\theta \\ \sin\theta & \cos\theta \end{bmatrix} \end{aligned} \tag{3.49}$$

For instance, $H(\boldsymbol{e}_x)$ and $H(\boldsymbol{e}_y)$ express correlation in the direction parallel and perpendicular to the local director, respectively. The numerical data for the standard parameter are shown in Fig.3.5. The plotted range is $R \geq \xi$. We see that the correlation tendency described in Fig.3.2 extends over several times of the correlation length. The depolarized scattering intensity $I(\boldsymbol{q})$, is also shown in Fig.3.5. Although not clear from the figure, the intensity is a monotonously decreasing function of the wavenumber along the q_x and q_y axes; there were no peaks at finite wave-numbers, in contrast to the experimental observation [15,

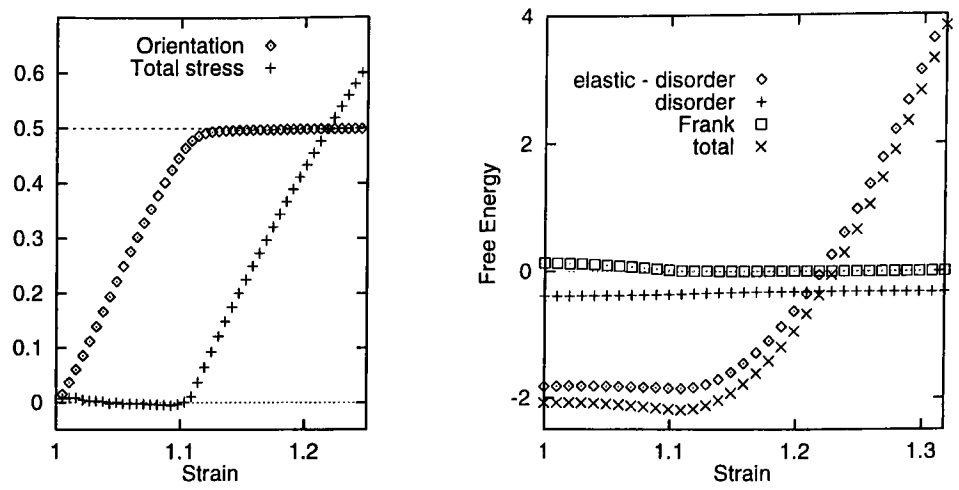

Figure 3.6: Left : Macroscopic orientation $\overline{Q}_{xx} = \overline{\cos^2\theta}/2$ and total stress $\sigma = \partial f/\partial\lambda_{||}$ as functions of $\lambda_{||}$. The stress is plotted in an arbitrary unit. Right : Free energy densities. The elastic free energy density is measured from μ. See the text for the definition of the disorder contribution.

19].

3.3 Polydomain-Monodomain transition

3.3.1 Numerical Simulation

Next we simulated the polydomain-monodomain transition using the non-linear elasticity model Eq.(2.35). In addition to Eq.(3.44) for the director, we solved the Langevin equation,

$$\frac{\partial \boldsymbol{u}}{\partial t} = -\Gamma_u \frac{\delta F}{\delta \boldsymbol{u}} + \boldsymbol{\eta}_u, \tag{3.50}$$

for the internal displacement $\boldsymbol{u} = \boldsymbol{r} - \overline{\lambda}\ \boldsymbol{r}_0$. After an equilibration stage at the polydomain state with $\lambda_{||} = 1$, we added an external stretching in the following way. An increment of strain $\lambda_{||} \to \lambda'_{||} = \lambda_{||} + \Delta\lambda_{||}$ was performed in two steps; (i) increase $\lambda_{||}$ at a constant rate and with thermal noise, until arriving at $\lambda'_{||}$. (ii) turn off the thermal noise for some time to approach the free energy minimum at $\lambda'_{||}$. This was iterated to obtain the free energy as a function of $\lambda_{||}$. The data shown below are for the parameters $K_F = 4, \mu = 100, \alpha = 0.4$, and $\gamma = 0.05$, unless otherwise stated. For this parameter $D = 0.5$, $M = 4$

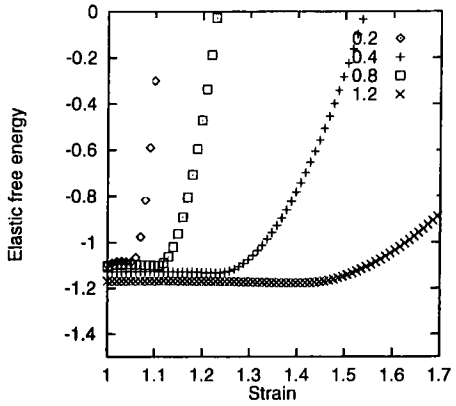

Figure 3.7: Elastic free energy density Δf_{el} divided by $\mu\alpha^2/8$ for $\alpha = 0.2, 0.4, 0.8$,and 1.2. For these values $\lambda_s = 1.05, 1.11, 1.24$, and 1.41, respectively.

and $\xi/\xi_c \sim 3$. The macroscopic orientation $\overline{Q}_{xx} = \overline{\cos^2\theta}/2$ and the macroscopic stress $\sigma = df/d\lambda_{||}$ are shown in Fig.3.6. The orientation shows a linear rise until saturating at $\lambda_{||} \simeq \lambda_s (= 1.11)$, while the stress is almost zero in the polydomain region $1 < \lambda_{||} < \lambda_s$, and linearly rises in the monodomain region $\lambda_{||} > \lambda_s$. The components of the free energy density are also shown in Fig.3.6. We define the disorder contribution F_{dis} to the elastic free energy by

$$F_{dis} = \frac{\mu}{2} \int dr (\delta_{ij} - \alpha Q_{ij}) P_{kl} \lambda_{ik} \lambda_{jl}. \tag{3.51}$$

Both F_{dis} and $F_{el} - F_{dis}$ are almost constant in the polydomain region, and the slightly negative slope of the total free energy is due to the Frank contribution. Next we varied the coupling constant α with keeping the values of D,M, and K_F fixed. Shown in Fig.3.7 is the elastic free energy density ΔF_{el} divided by $\mu\alpha^2/8$. In the weak disorder limit it should be $-1 + O(\alpha^3)$ from the previous analysis. The slope of the free energy is only slightly negative and is almost independent of α. We also find that the crossover to monodomain occurs at strain slightly larger than λ_s. This can be attributed to hysteresis; when we decreased $\lambda_{||}$ from the monodomain region, the crossover occurred at slightly below λ_s.

3.3.2 Scattering intensity

In Fig.3.8 we show the depolarized scattering intensity. In contrast to Fig.3.5, the intensity develops peaks at finite wave-numbers. This is quite probably an artifact of our numerical scheme : the elastic displacement obeys a diffusive

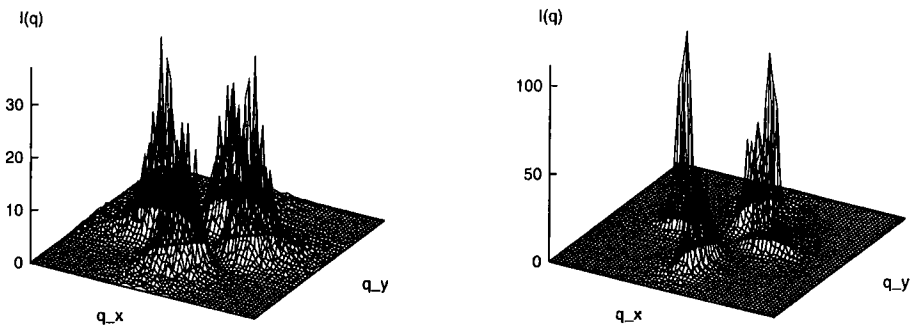

Figure 3.8: Depolarized scattering intensity $I(\mathbf{q}) = \langle |Q_{xy}(\mathbf{q})|^2 \rangle$. Average is taken over 10 samples for each parameter. Left : $\lambda_{\parallel} = 1.0$. Right : $\lambda_{\parallel} = 1.06$. Peaks in the direction parallel to the stretching axis are higher and narrower than those in the perpendicular direction.

equation Eq.(3.50) and relaxes very slowly at long wavelengths, although we do not yet well understand how it affects the order parameter. Under stretching, the peaks on the q_x-axis become higher than those on the q_y-axis, and the latter are broader than the former. These are just the opposite to the experimental observation [15, 19]. At the moment the source of this discrepancy remains puzzling. For instance, it is not clear whether our 2D result can be used to interpret the experimental data, which are obtained from freely-suspended films. It is also to be noted that the peak intensity increases by stretching. This feature agrees with the experiment, where the unstretched state was opaque and the scattering pattern was not detectable.

3.3.3 Quasi-soft elasticity

Let us summarize the mechanical response of an isotropically crosslinked network. In the previous section, we have seen that the soft response originates from re-configuration of the domain structure, which is illustrated in Fig.3.2 and gives rise to the "four-leaf clover" scattering. We have obtained a vanishingly small stress even for a sizable value of α. We shall call the soft response *quasi-soft elasticity*, in order to distinguish it from the *soft elasticity* [10] of homogeneous and clean networks. Very recently, a conflicting argument was presented by Fridrikh and Terentjev [22], who claimed that the P-M transition costs a positive

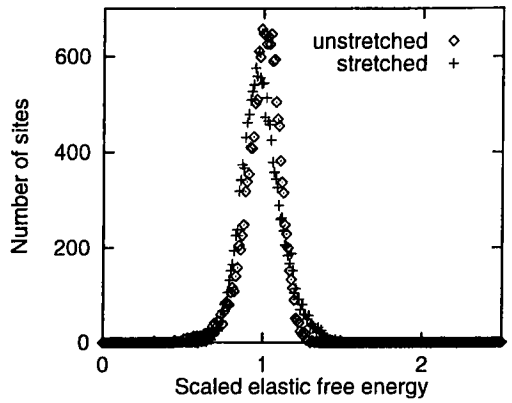

Figure 3.9: Distribution of elastic free energy contained in a single site. The horizontal axis indicates the elastic free energy Δf_{el} divided by its spatial average. Cases with and without stretching ($\lambda_{\|} = 1.0$ and $\lambda_{\|} = 1.06$) are shown.

elastic free energy of $O(\alpha^2)$. Their basic picture is that the elastic free energy is localized at "domain walls" by stretching, while inside each domain the strain and order parameter are homogeneous. However, our analysis and numerical data show that this is not the case. Plotted in Fig.3.9 is the distribution of elastic free energy contained in a single site. It has a single sharp peak, and is only slightly changed by stretching. This implies that the director and local strain axis coincidently (and graduately) rotate toward the external force direction, as the strain is increased (see Fig.3.10). This may be called a quasi-Goldstone mode (but is not a genuine Goldstone mode because of the quenched disorder and the anharmonic correction). The quasi-Goldstone mode originates from the I-N transition-induced deformation. Although our results are for the 2D case, we believe that the theoretical picture of the quasi-soft elasticity remains valid in the 3D case.

3.3.4 Crosslinking in the nematic phase

Next we consider the case where the crosslinking was done in a polydomain nematic state (Case II). The initial orientational configuration was prepared by simulating a simplified model of the phase ordering kinetics of nematic polymer melts; starting with a spatially uncorrelated initial configuration, we solved Eq.(3.44) with $\mu = 0$, $\alpha = 0$, and $\eta = 0$ until the domain grows to a size larger than ξ_c (Case II-B). Then the order parameter configuration is copied to $Q^0_{ij}(\boldsymbol{r})$,

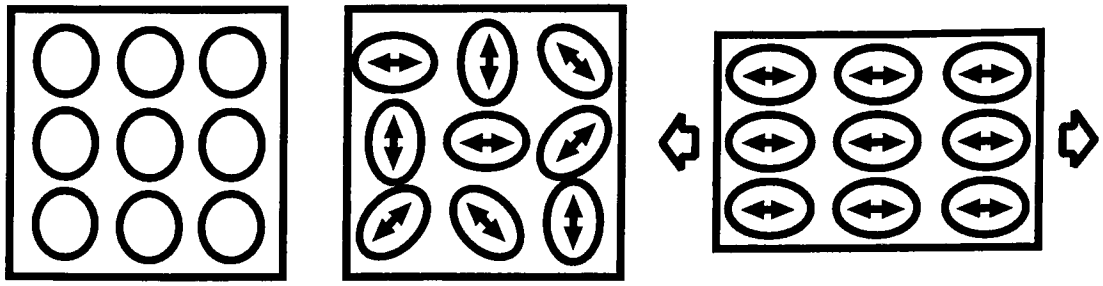

Figure 3.10: Schematic illustration of the quasi-Goldstone mode (in a macroscopic view over many domains.) The soft response is due to simultaneous rotation of the strain axis (indicated by ellipses) and the director.

and we have solved Eqs.(3.44) and (3.50) with the designated values of μ and α for some more time to equilibrate the system. As shown in Fig.3.11, the macroscopic stress has a finite positive slope in the polydomain region. From Fig.3.12 we see that the free energy has a uniform spatial distribution at $\lambda_{||} = 1$, which is broadened by stretching. These reflect the fact that Q_{ij} is almost equal to Q^0_{ij} at $\lambda_{||} = 1$, and Q^0_{ij} acts as a correlated random field that produces a strong resistance against stretching.

3.4 Fluctuation in the Monodomain State

3.4.1 Soft mode

By stretching the network after or in the course of crosslinking, we can obtain a nearly homogeneous monodomain state. Golubović and Lubensky [6] considered a general model of non-linear elasticity whose linear elastic moduli can be negative. When the shear modulus becomes negative, the system undergoes a spontaneous elongation. They showed that, in this ground state, there are soft thermal phonon modes with $\langle |\boldsymbol{u}(\boldsymbol{q})|^2 \rangle \propto q^{-4}$. They also considered the effect of random internal stresses in a harmonic approximation, and suggested a further softening $\langle |\boldsymbol{u}(\boldsymbol{q})|^2 \rangle \propto q^{-6}$ on a plane in the $\boldsymbol{q}$- space. Their results can be translated in terms of nematic gels originally crosslinked in the isotropic phase. However, since their model does not contain the nematic order parameter, it has not been clear whether their results are indeed valid in nematic

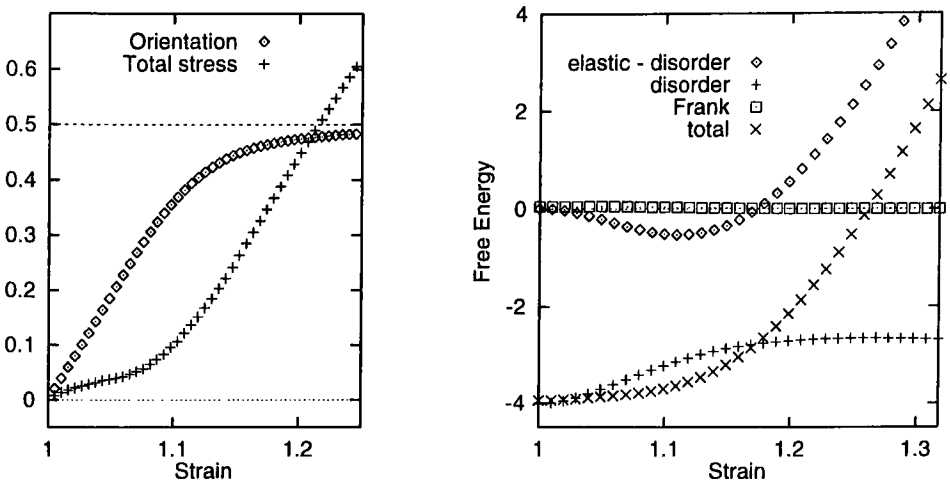

Figure 3.11: Left : Macroscopic orientation $\overline{Q}_{xx} = \overline{\cos^2\theta}/2$ and total stress $\sigma = \partial F/\partial\lambda_{\|}$. Crosslinking was made in a polydomain nematic state. Right : Free energy densities. The disorder contribution is defined by Eq.(3.51) with P_{ij} replaced by $\alpha_0 Q^0_{ij}$.

gels. Fluctuations in networks crosslinked in a monodomain nematic state was first analyzed by Olmsted. Using the extended affine deformation theory, he showed that the director and strain possess soft modes of thermal fluctuation with $\langle|\delta\boldsymbol{n}(\boldsymbol{q})|^2\rangle \propto q^{-2}$ and $\langle|\boldsymbol{u}(\boldsymbol{q})|^2\rangle \propto q^{-4}$, respectively. The existence of soft director fluctuation implies that the monodomain state is unstable to a buckling of the director for an arbitrary small compression along the director. This has been experimentally observed [41] and called the stripe instability. However, he did not treat the case of isotropic crosslinking, and the effect of crosslinking condition has remained unknown.

The purpose of this section is twofold. In this subsection, first we generalize the result of Olmsted by showing that clean nematic gels in the ground state $\lambda_{\|} = \lambda_s$ have soft modes of director fluctuation, regardless of the crosslinking condition. Secondly, we discuss the effect of quenched disorder on the director fluctuation. We study two types of quenched disorder, i.e., inhomogeneous director configuration at the moment of crosslinking, and the random stresses. We consider networks almost completely aligned in the x-direction;

$$\boldsymbol{n} \;=\; \boldsymbol{e}_x + \delta\boldsymbol{n}.$$

We assume the crosslinking to be done either in the isotropic phase, or in the

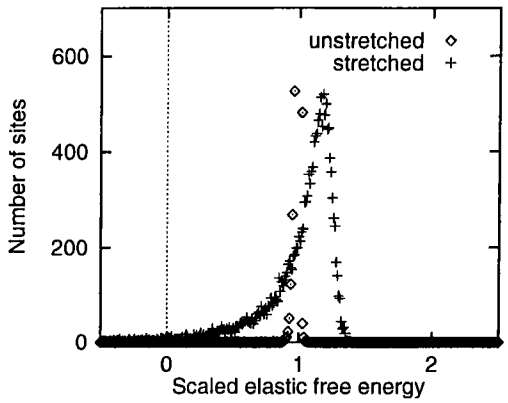

Figure 3.12: Distribution of elastic free energy contained in a single site, in a system crosslinked in the nematic phase. Cases with and without stretching ($\lambda_{\|} = 1.0$ and $\lambda_{\|} = 1.06$) are shown. The peak for the unstretched case counts about 5000 sites and is far out of the plotted range.

nematic phase with an almost uniform configuration

$$\boldsymbol{n}_0 = \boldsymbol{e}_x + \delta \boldsymbol{n}_0. \tag{3.52}$$

Now we derive the long-range elastic interaction between director fluctuations. To this end, it is convenient to reparametrize the chain conformation tensors as

$$\ell^0_{ij} = \tilde{\ell}^0_e L^0_{ij} = \tilde{\ell}^0_e(\delta_{ij} + \beta_0 n^0_i n^0_j + \tilde{P}_{ij}), \tag{3.53}$$

$$\ell_{ij} = \tilde{\ell}_e L_{ij} = \tilde{\ell}_e(\delta_{ij} + \beta\, n_i n_j), \tag{3.54}$$

where β and β_0 characterize the equilibrium chain anisotropy and $\tilde{P}_{ij}$ is the nonequilibrium contribution (random stress). The basic free energy Eq.(2.35) is rewritten as

$$F_{el} = \frac{\tilde{\mu}}{2} \int d\boldsymbol{r}\, L^{-1}_{ij} L^0_{kl} \lambda_{ik} \lambda_{il}, \tag{3.55}$$

$$\tilde{\mu} = K_B T \tilde{\ell}^0_e \tilde{\ell}^{-1}_e$$

Hereafter we denote $\tilde{\mu}$ and $\tilde{P}_{ij}$ simply as μ and P_{ij}. The spontaneous elongation is expressed as

$$\lambda_s = \left(\frac{1+\beta}{1+\beta_0}\right)^{(d-1)/2d} \tag{3.56}$$

For the computation it is also convenient to introduce the quantity

$$C_{ij} = L^0_{kl} \overline{\lambda}_{ik} \overline{\lambda}_{jl}, \tag{3.57}$$

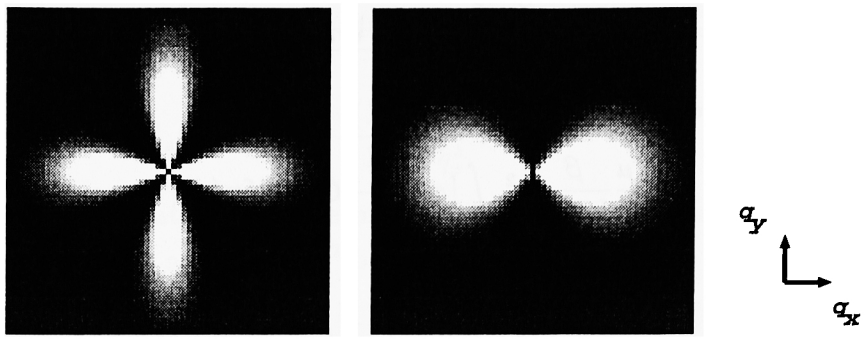

Figure 3.13: Amplitudes of thermal fluctuation at the threshold $\lambda_{\|} = \lambda_s$. Plotted are $\langle|\delta n_y(\mathbf{q})|^2\rangle$ (left) and $\langle|\delta n_z(\mathbf{q})|^2\rangle$ (right) for $\beta = 0.1$ and on the q_x-q_y plane.

with which the elastic free energy can be expanded as

$$F_{el} = \frac{\mu}{2}\int dr\Big[C_{ij}L^{-1}_{ij} + 2C_{ik}L^{-1}_{jk}(\partial_i u_j) + \overline{C}_{ij}\overline{L}^{-1}_{kl}(\partial_i u_k)(\partial_j u_l) + \frac{K}{2}(\partial_i u_i)^2\Big]. \tag{3.58}$$

In the third term of the integrand we have replaced C_{ij} and L^{-1}_{ij} by their spatial averages as the deviations will contribute only to higher order terms in the effective free energy. Solving the mechanical equilibrium condition $\delta F_{el}/\delta \boldsymbol{u} = 0$ and taking the incompressible limit $K \to \infty$, we obtain

$$\boldsymbol{u}(\boldsymbol{q}) = \frac{1}{\overline{C} : \boldsymbol{qq}}\Big[L\cdot\boldsymbol{g}(\boldsymbol{q}) - \frac{\boldsymbol{q}\ \ L\cdot\boldsymbol{g}(\boldsymbol{q})}{L:\boldsymbol{qq}}L\cdot\boldsymbol{q}\Big], \tag{3.59}$$

where

$$g_i = \partial_j(C_{jk}L^{-1}_{ik}). \tag{3.60}$$

The effective free energy is given by

$$F_{el} = \frac{\mu}{2}\int dr\ C : L^{-1} + \frac{\mu}{2}\int_{\boldsymbol{q}} \frac{1}{\overline{C}:\boldsymbol{qq}}\Big[\frac{1}{\overline{L}:\boldsymbol{qq}}\Big|\boldsymbol{q}\ \ \overline{L}\cdot\boldsymbol{g}(\boldsymbol{q})\Big|^2 - \boldsymbol{g}(\boldsymbol{q})\ \ \overline{L}\ \ \boldsymbol{g}(-\boldsymbol{q})\Big]. \tag{3.61}$$

Soft mode

First we assume that the initial crosslinking was done in a perfectly uniform state $\lambda^0_{ij} = \delta_{ij}, \delta n^0_i = 0$. Substituting $C_{ij} = \overline{C}_{ij}$ and

$$g_i(\boldsymbol{q}) = \sqrt{-1}\ q_j\overline{C}_{jk}(\delta L^{-1})_{ik}$$

$$= -\sqrt{-1}\,\frac{\beta}{1+\beta}\left[\lambda_\perp^2\delta_{ix}\boldsymbol{q}\cdot\delta\boldsymbol{n}(\boldsymbol{q})+(1+\beta_0)\lambda_\parallel^2 q_x\delta n_i(\boldsymbol{q})\right] \quad (3.62)$$

into Eq.(3.61), we obtain

$$F_{el} = \frac{\mu}{2}\frac{\beta}{1+\beta}\lambda_\perp^2\int_{\boldsymbol{q}}[\rho-1-G(\hat{\boldsymbol{q}})]|\delta\boldsymbol{n}(\boldsymbol{q})|^2+\text{const.} \quad (3.63)$$

where

$$G(\boldsymbol{q}) = \frac{\beta}{1+\beta}\frac{\left[1+\beta-\dfrac{(1+\beta+\rho)^2\hat{q}_x^2}{1+\beta\hat{q}_x^2}\right]\hat{q}_\parallel^2+\rho^2\hat{q}_x^2}{1+(\rho-1)\hat{q}_x^2}, \quad (3.64)$$

$$\hat{q}_\parallel = \frac{|\hat{\boldsymbol{q}}\cdot\delta\boldsymbol{n}(\boldsymbol{q})|}{|\delta\boldsymbol{n}(\boldsymbol{q})|},$$

and

$$\rho = \frac{(1+\beta_0)\lambda_\parallel^2}{\lambda_\perp^2} \quad (3.65)$$

The $\rho-1$ in the square bracket of Eq.(3.63) has its origin in the first integral of Eq.(3.61). This term always tends to align the director in the stretching direction. In the case of nematic crosslinking ($\beta_0>0$), the aligning effect remains even without stretching ($\lambda_\parallel=\lambda_\perp=1$). If the maximum value of $G(\hat{\boldsymbol{q}})$ exceeds $\rho-1$, the monodomain state is unstable to director buckling. It can be shown that

$$\begin{array}{lllll} G_{max}=\dfrac{\rho\beta}{1+\beta} & \text{attained at} & \hat{\boldsymbol{q}}\parallel\boldsymbol{e}_x & \text{for} & \rho\geq 1+\beta, \\ G_{max}=\beta & \text{attained at} & \hat{\boldsymbol{q}}\parallel\delta\boldsymbol{n}(\boldsymbol{q}) & \text{for} & \rho\leq 1+\beta. \end{array}$$

which tells us that the stability threshold is located at $\rho=\rho_c=1+\beta$ or equivalently at $\lambda_\parallel=\lambda_s$, where the bend fluctuation ($\boldsymbol{q}\parallel\overline{\boldsymbol{n}}$) and the splay fluctuation ($\boldsymbol{q}\parallel\delta\boldsymbol{n}$) are both marginally stable. If we assume that the wave-vector lies in the x-y plane, the amplitude of thermal fluctuation at the threshold is given by

$$|\delta n_i(\boldsymbol{q})|^2 = \frac{k_BT}{\dfrac{\mu\beta^2}{1+\beta}\lambda_\perp^2 A_i(\hat{\boldsymbol{q}})+Kq^2} \quad (i=y,z), \quad (3.66)$$

$$A_y(\hat{\boldsymbol{q}}) = 1-\frac{(1+\beta)\hat{q}_x^2+s(\hat{\boldsymbol{q}})\hat{q}_y^2}{1+\beta\hat{q}_x^2}, \quad (3.67)$$

$$s(\hat{\boldsymbol{q}}) = 1 - \frac{4(1+\beta)\hat{q}_x^2}{1+\beta\hat{q}_x^2}, \tag{3.68}$$

$$A_z(\hat{\boldsymbol{q}}) = 1 - \frac{(1+\beta)\hat{q}_x^2}{1+\beta\hat{q}_x^2}. \tag{3.69}$$

It is noteworthy that $A_i(\hat{\boldsymbol{q}})$'s are independent of the crosslinking condition β_0. At $\hat{q}_x = 0$, $|\delta n_y(\hat{\boldsymbol{q}})|^2$ and $|\delta n_z(\hat{\boldsymbol{q}})|^2$ both diverge in the limit $q \to 0$. Furthermore, for any unit vector $\boldsymbol{e}$ lying in the $y-z$ plane, $\langle|\boldsymbol{e}\ \ \delta\boldsymbol{n}(\boldsymbol{q})|^2\rangle = (\boldsymbol{e}\cdot\boldsymbol{e}_y)^2|\delta n_y(\hat{\boldsymbol{q}})|^2 + (\boldsymbol{e}\ \ \boldsymbol{e}_z)^2|\delta n_z(\hat{\boldsymbol{q}})|^2$ diverges at $\hat{q}_x = 0$. Thus, all the modes on the plane $\boldsymbol{q} \perp \overline{\boldsymbol{n}}$ except for the line $\boldsymbol{q} \perp \delta\boldsymbol{n}$ are free from the rubber-elastic effect. The amplitudes for $\beta = 0.1$ are plotted in Fig.3.13.

3.4.2 Effect of quenched disorder

Initital director inhomogeneity

Now let us move to the effect of quenched disorder. To make things simple, we shall limit our calculation to the case with $\beta_0 = \beta$ and $\lambda_{||} = \lambda_s = 1$. First we consider the effect of quenched director inhomogeneity. The only alteration in the derivation of the effective free energy is to replace Eq.(3.62) by

$$\begin{aligned} g_i(\boldsymbol{q}) &= \sqrt{-1}\, q_j[\overline{C}_{jk}(\delta L^{-1})_{ik} + (\delta C_{jk})\overline{L}_{ik}^{-1}] \\ &= -\sqrt{-1}\left[\frac{\beta}{1+\beta}\delta_{ix}\boldsymbol{q}\cdot\delta\boldsymbol{m}(\boldsymbol{q}) + \beta q_x \delta m_i(\boldsymbol{q})\right], \end{aligned} \tag{3.70}$$

where

$$\delta\boldsymbol{m} = \delta\boldsymbol{n} - \delta\boldsymbol{n}_0. \tag{3.71}$$

Putting it into Eq.(3.61), we have the effective free energy

$$F_{el} = \frac{\mu}{2}\frac{\beta}{1+\beta}\int_{\boldsymbol{q}}[\beta - G_m(\hat{\boldsymbol{q}})]|\delta\boldsymbol{m}(\boldsymbol{q})|^2, \tag{3.72}$$

where $G_m(\hat{\boldsymbol{q}})$ is equal to $G(\hat{\boldsymbol{q}})$ (in Eq.(3.64)) but with $\rho = 1+\beta$ and with $\hat{q}_{||}$ redefined as

$$\hat{q}_{||} = \frac{|\hat{\boldsymbol{q}}\cdot\delta\boldsymbol{m}(\boldsymbol{q})|}{|\delta\boldsymbol{m}(\boldsymbol{q})|}. \tag{3.73}$$

Generally, in the presence of quenched disorder, the director fluctuation consists of two parts, as

$$\delta\boldsymbol{n} = \delta\boldsymbol{n}_{st} + \delta\boldsymbol{n}_{th}. \tag{3.74}$$

The first part $\delta \boldsymbol{n}_{st}$ is a static fluctuation determined by minimizing the free energy, while $\delta \boldsymbol{n}_{th}$ stands for the thermal fluctuation around the shifted optical axis $\overline{\boldsymbol{n}} + \delta \boldsymbol{n}_{st}$. The total fluctuation amplitude is given by

$$\left\langle |\delta \boldsymbol{n}(\boldsymbol{q})|^2 \right\rangle = \left\langle |\delta \boldsymbol{n}_{st}(\boldsymbol{q})|^2 \right\rangle + \left\langle |\delta \boldsymbol{n}_{th}(\boldsymbol{q})|^2 \right\rangle \tag{3.75}$$

The situation is analogous to the case of density fluctuation in inhomogeneous isotropic gels, discussed in Section 2.1.2. In the present case, from Eq.(3.72) we have $\delta \boldsymbol{n}_{st} = \delta \boldsymbol{n}_0$ except in the soft directions $\boldsymbol{q} \parallel \overline{\boldsymbol{n}}$ or $\boldsymbol{q} \parallel \delta \boldsymbol{n}_0$. On the other hand, there is no effect of the quenched director inhomogeneity in the soft directions.

Random stresses

Next we consider the effect of random stresses. We assume the Case I; the network is crosslinked in the isotropic phase and $\beta_0 = 0$. Then, from symmetry, P_{ij} has a distribution of the form Eq.(2.9). After some calculation, we obtain the effective free energy at $\lambda_{\parallel} = \lambda_s$ as

$$\begin{aligned} F_{el} \;=\; & \frac{\mu}{2}\frac{\beta^2}{(1+\beta)^{4/3}} \int_{\boldsymbol{q}} \Bigg\{ \left| \delta n_i(\boldsymbol{q}) \right|^2 - 2\delta n_i(\boldsymbol{q}) \delta \hat{C}_{ix}(-\boldsymbol{q}) \\ & - \frac{1}{1+\beta \hat{q}_x^2} \Bigg[\left| \hat{q}_i \delta n_i(\boldsymbol{q}) - \hat{q}_i \delta \hat{C}_{ix}(\boldsymbol{q}) \right|^2 \\ & + (1+\beta) \left| \hat{q}_x \delta n_i(\boldsymbol{q}) - \hat{q}_j \delta \hat{C}_{ji}(\boldsymbol{q}) \right|^2 \\ & - \frac{1+\beta}{1+\beta \hat{q}_x^2} \left| 2\hat{q}_x \hat{q}_i \delta n_i(\boldsymbol{q}) - \hat{q}_i \hat{q}_j \delta \hat{C}_{ij}(\boldsymbol{q}) \right|^2 \Bigg] \Bigg\} \\ & + \text{const.} \end{aligned} \tag{3.76}$$

where

$$\delta \hat{C}_{ij} = \beta^{-1}(C_{ij} - \overline{C}_{ij}). \tag{3.77}$$

In the long-wavelength limit, the Frank elasticity is negligible and the static fluctuation $\delta \boldsymbol{n}_{st}$ is determined by solving

$$\frac{\delta F_{el}}{\delta \boldsymbol{n}} = 0, \tag{3.78}$$

which yields

$$\delta n_{st,i}(\boldsymbol{q}) \;=\; \frac{1}{1-\hat{q}_x^2} \left\{ (1+\beta \hat{q}_x^2) \delta \hat{C}_{ix}(\boldsymbol{q}) \right.$$

$$
\begin{aligned}
&-\frac{\hat{q}_i}{\hat{q}_x^2}\cdot\Omega(\hat{q}_x)\Bigg[\beta\hat{q}_x^2\hat{q}_j\delta\hat{C}_{jx}(\boldsymbol{q})-(1+\beta)\left(1-\frac{2}{1+\beta\hat{q}_x^2}\right)\hat{q}_x\hat{q}_j\hat{q}_k\delta\hat{C}_{jk}(\boldsymbol{q})\Bigg]\\
&-(1+\beta)\hat{q}_x\hat{q}_j\delta\hat{C}_{ji}(\boldsymbol{q})\\
&-\hat{q}_i\left[\hat{q}_j\delta\hat{C}_{jx}(\boldsymbol{q})-\frac{2(1+\beta)\hat{q}_x}{1+\beta\hat{q}_x^2}\hat{q}_j\hat{q}_k\delta\hat{C}_{jk}(\boldsymbol{q})\right]\Bigg\},
\end{aligned}
\tag{3.79}
$$

with

$$
\Omega(\hat{q}_x)=1+\frac{1-\hat{q}_x^2}{1-\dfrac{(1+\beta\hat{q}_x^2)}{4(1+\beta)}}.
\tag{3.80}
$$

Let us restrict our attention to the soft modes. For the mode with $\hat{\boldsymbol{q}}=\boldsymbol{e}_x$, the overall factor $1/(1-\hat{q}_x^2)$ in Eq.(3.79) diverges while its multiplicand $\{\cdots\}$ does not vanish. For the second class of modes with $\hat{\boldsymbol{q}}\perp\boldsymbol{e}_x$ and with $\hat{\boldsymbol{q}}\quad\delta\boldsymbol{n}\neq 0$, the factor $\hat{q}_i/\hat{q}_x^2$ in the second line of Eq.(3.79) diverges while its multiplicand is finite. This means that the random stresses act on the soft modes, in contrast to the initial director inhomogeneity. Incorporating the Frank elasticity, these modes have finite amplitudes which go as

$$
\delta n_{st,i}(\boldsymbol{q})=\frac{\mu}{Kq^2}T_{ijk}(\hat{\boldsymbol{q}})\delta\hat{C}_{jk}(\boldsymbol{q})+O(q^{-4})
\tag{3.81}
$$

in the long wavelength, where T_{ijk} is a certain non-dimensional tensor. For these modes, the total square amplitude is the sum of

$$
\left\langle|\delta\boldsymbol{n}_{st}(\boldsymbol{q})|^2\right\rangle\sim\frac{\mu^2}{K^2q^4}\gamma^2
\tag{3.82}
$$

and

$$
\left\langle|\delta\boldsymbol{n}_{th}(\boldsymbol{q})|^2\right\rangle\sim\frac{k_BT}{Kq^2}.
\tag{3.83}
$$

The static fluctuation dominates the thermal one for $q\lesssim q_{st}=\mu\gamma/\sqrt{Kk_BT}$ For flexible LCPs we have $K\sim k_BTa^2$ where $a\sim 1nm$ is the monomer size. We also have $\mu\sim k_BT\nu_0\sim k_BT/\xi_m^3$ where $\xi_m\sim 10^2a$ is the mesh size of the network. This leads to an estimate

$$
q_{st}^{-1}\sim a\cdot(\xi_m/a)^{3/2}/\sqrt{\nu_0\gamma^2}\sim 10^3/\sqrt{\nu_0\gamma^2}\,nm.
\tag{3.84}
$$

For a strongly disordered network with $\nu_0\gamma^2\gtrsim 1$, the static contribution to the light scattering intensity cannot be negligible. It can be also shown that the strain fluctuation obtains a static part $\langle|\boldsymbol{u}(q)|^2\rangle\propto q^{-6}$ on the plane $\boldsymbol{q}\perp\overline{\boldsymbol{n}}$ in the $\boldsymbol{q}$-space due to the random stresses, as Golubović and Lubensky showed.

Chapter 4

Summary

Let us summarize the results and discuss future directions. We have modeled the quenched random stresses in nematic gels within the affine-deformation theory of rubber-elasticity. In a harmonic approximation, we have derived the explicit form of the long-range interaction of the orientational order parameter, with itself and with the random stresses. In the nematic phase, the random stresses act on the director both locally and non-locally, resulting in the polydomain state. We have pointed out the importance of crosslinking conditions. For networks originally crosslinked in the isotropic phase, the I-N transition induces a heterogeneous spontaneous deformation along the director. The domain structure is rearranged due to the long-range interaction, resulting in a significant free energy reduction. This leads to an anomalously soft mechanical response with a slight change of $O(\alpha^3)$ in the elastic free energy. By numerical simulation, we have obtained soft responses even for a sizable value of α. The domain rearrangement also partially explains the "four-leaf clover"-type anisotropy observed in depolarized scattering experiments. However, the direction of the stretching-induced anisotropy in the intensity is opposite to the experiment. The correlation length is determined mainly by the balance between the Frank elastic and random stress effect, and has an exponential dependence on the disorder strength. The correlation function decays nearly exponentially for a strong quenched disorder and faster for a weaker one, in agreement with previous results for the random-field 2D XY model.

We also studied the effect of random stresses on fluctuations in the monodomain state, which is unstable below a critical stretching ratio. The soft fluctuation at the instability threshold is enhanced by random stresses.

Finally we suggest some possible extensions of this work. First of all, dynamical aspects have been completely neglected in the present work. Very recently, there appeared a few experimental indications of glass-like slow dynamics in nematic gels. A non-exponential slow relaxation of the plateau stress has been observed [18], which shows that the system cannot reach its true thermal equilibrium in a realistic time-scale of observation. A non-exponential decay is also observed in the dynamic correlation function in the monodomain state, with use of dynamic light scattering [42]. The unusual hole in the depolarized scattering intensity, observed at long-wavelengths, may also be understood as the result of a slow relaxation, as our numerical simulation (with an artificial dynamics) tentatively suggested. We should construct a dynamical model and analyze the effect of random quenched disorder. We may also pursue an analogy with other disordered systems with slow dynamics, such as liquid crystals in porous media [43] and random walks in a random potential [44].

Secondly, we are investigating phase separation in nematic gels. The volume mismatch between the two phases produces a shear strain at the phase boundary, which orients the director parallel to the interface through the strain-orientation coupling. This may result in a strong resistance of the director against an external electric field. Dispersions of liquid crystals in gels have been extensively studied for application in electro-optical devices [45], and micro-phase-separated nematic gels have also been realized [46]. We wish that experiments from a physical point of view will be conducted in a near future. Effects of strain-orientation coupling, as transient phenomena, may also be observed in viscoelastic liquid-crystalline polymer solutions.

Acknowledgement

The author is greatly indebted to Professor Akira Onuki for helpful discussions, written correspondences and critical readings of manuscripts throughout the course. The present study, in its point of view, owes very much to his work on elastic effects in metallic solids and gels. The author thanks Dr. Eugene Terentjev, Dr. Jun Yamamoto, and Dr. Alexandra ten Bosch for invaluable and specialized comments and discussions. Thanks are also due to many other people for discussions on the present and other topics, and for help in daily work.

Bibliography

[1] S. Alexander, J. Phys. (France) **45**, 1939 (1984).

[2] For a review, see : M. Shibayama, Macromol. Chem. Phys. **199**, 1 (1998).

[3] H. Finkelmann, H. J. Koch and G. Rehage, Macromol. Rapid Commun. **2**, 317 (1981).

[4] For a review of early experiments, see : G. G. Barklay and C. K. Ober, Prog. Polym. Sci. **18**, 899 (1993).

[5] P G. de Gennes, C. R. Acad. Sci. **B281**, 101 (1975)

[6] L. Golubović and T. C. Lubensky, Phys. Rev. Lett. **63**, 1082 (1989).

[7] M. Warner, K. P. Gelling, and T. A. Vilgis, J. Chem. Phys. **88**, 4008 (1988).

[8] S. S. Abramochuk and A. R. Khokhlov, Doklady. Akademii. Nauk. SSSR. (Doklady Phys. Chem) **297**, 385 (1987).

[9] P. J. Flory, Principles of Polymer Chemistry, (Cornell University Press, Ithaca, 1953)

[10] M. Warner, P. Bladon, and E. M. Terentjev J. Phys. II France 4, 93 (1994).

[11] For a review, see : M. Warner and E. M. Terentjev, Prog. Polym. Sci. **21**, 853 (1996).

[12] P. D. Olmsted, J. Phys. II France **4**, 2215 (1994).

[13] J. Schätzle, W. Kaufhold, and H. Finkelmann, Macromol. Chem. **190**, 3269 (1989).

[14] J. Küpfer and H. Finkelmann, Macromol. Chem. Phys. **195**, 1353 (1994).

[15] S. M. Clarke, E. M. Terentjev, I. Kundler and H. Finkelmann, Macromolecules **31**, 4862 (1998).

[16] G. H. F. Bergmann, H. Finkelmann, V. Percec and M. Zhao, Macromol. Rapid. Commun. **18**, 353 (1997).

[17] E. R. Zubarev, R. V. Talroze, T. I. Yuranova, N. A. Plate, and H. Finkelmann, Macromolecules **31**, 3566 (1998).

[18] S. M. Clarke and E. M. Terentjev, Phys. Rev. Lett. **81**, 4436 (1998).

[19] S. M. Clarke, E. Nishikawa, H. Finkelmann and E. M. Terentjev, Macromol. Chem. Phys. **198**, 3485 (1997).

[20] A. ten Bosch and L. Varichon, Macromol. Theor. Simul. **3**, 533 (1994).

[21] S. V. Fridrikh and E. M. Terentjev, Phys. Rev. Lett. **79**, 4661 (1997).

[22] S. V. Fridrikh and E. M. Terentjev, Phys. Rev. E. **60**, 1847 (1999).

[23] L. D. Landau and E. M. Lifshitz, Theory of Elasticity, 3rd Edition (Pergamon, Oxford, 1986).

[24] For a review, see : P Nozieres, in Solids Far From Equilibrium, edited by C. Godrèche (Cambridge University Press, Cambridge) p. 1.

[25] A. J. Ardell, R. B. Nicholson and J. D. Eshelby, Acta Metall. **14** 1295 (1966).

[26] J. W. Cahn, Acta Metall. **9**, 795 (1961).

[27] A. Onuki, J. Phys. Soc. Japan. **58**, 3065 (1989).

[28] A. Onuki, J. Phys. Soc. Japan. **58**, 3069 (1989).

[29] For a review, see : A. Onuki, in Adv. Polym. Sci. **109**, Responsible Gels : Volume Transitions I, edited by K. Dušek (Springer, Berlin, 1993), p.63.

[30] M. Goulian, R. Bruinsma, and P. Pincus, Europhys. Lett. **22**, 145 (1993).

[31] J. Bastide, L. Leibler and J. Prost, Macromolecules **23**, 1821 (1990).

[32] A. Onuki, J. Phys. II (France) **2**, 45 (1992).

[33] P G. de Gennes and J. Prost, The Physics of Liquid Crystals, 2nd Edition (Oxford University Press, Oxford, 1993).

[34] E. M. Chudonovsky, W. M. Saslow, and R. A. Serota, Phys. Rev. B **33**, 251.

[35] A. Maritan, M. Cieplak, and J. R. Banavar, in [45], p. 483.

[36] Y. Imry and S. -K. Ma, Phys. Rev. Lett. **35**,1399 (1975).

[37] M. J. P. Gingras and D. A. Huse, Phys. Rev. B **53**, 15193 (1996).

[38] Y. -K. Yu, P. L. Taylor and E. M. Terentjev, Phys. Rev. Lett. **81**, 128 (1998).

[39] B. Dieny and B. Barbara, Phys. Rev. B **41**, 11549 (1990).

[40] M. Doi and S. F Edwards, The Theory of Polymer Dynamics, (Oxford University Press, Oxford, 1986).

[41] I. Kundler and H. Finkelmann, Macromol. Chem. Rapid Commun., **16**, 679 (1995).

[42] Dr. Jun Yamamoto, private communication.

[43] X. I. Wu, W. I. Goldburg, M. X. Liu and J. Z. Xue, Phys. Rev. Lett. **69** 470 (1992).

[44] E. Marinari, G. Parisi, D. Ruelles and P. Windey, Phys. Rev. Lett **50**, 1223 (1983)

[45] Liquid Crystals in Complex Geometries Formed by Polymer and Porous Networks, edited by G. P. Crawford and S. Žumer, (Taylor and Francis, London, 1996).

[46] R. A. M. Hikmet and H. N. J. Boots , Phys. Rev. E **51**, 5824 (1994).